Cement and Concrete Composites 147 (2024) 105427

Contents lists available at ScienceDirect

Cement and Concrete Composites

journal homepage: www.elsevier.com/locate/cemconcomp

Alkaline activated cements obtained from ferrous and non-ferrous slags. Electric arc furnace slag, ladle furnace slag, copper slag and silico-manganese slag

M.A. Gómez-Casero [a,b], S. Bueno-Rodríguez [a,b], E. Castro [a,b], D. Eliche Quesada [a,b,*]

[a] Department of Chemical, Environmental, and Materials Engineering, Higher Polytechnic School of Jaén, University of Jaén, Campus Las Lagunillas s/n, 23071, Jaén, Spain

[b] Center for Advanced Studies in Earth Sciences, Energy and Environment (CEACTEMA), University of Jaén, Campus Las Lagunillas, s/n, 23071, Jaén, Spain

ARTICLE INFO

Keywords:
Ferrous slags
Non-ferrous slags
Silica modulus
Alkali activated cements
Mechanical properties

ABSTRACT

Ferrous slag: electric arc furnace slag (EAFS) and ladle furnace slag (LFS); and non-ferrous slag: copper slag (CS) and silicon-manganese slag (SiMnS) have been used as precursors for alkali activated cements (AACs). The objective of the study was to evaluate the effect of the silica modulus (Ms = SiO_2/K_2O) (0.5–1.8) of the potassium silicate/potassium hydroxide solution on the microstructure and technological properties of AACs using individual slags. The results obtained indicate that under the activation conditions used, CS and EAFS are more reactive slags, giving rise to AACs with optimum flexural and compressive strengths of 7.5 and 51.5 MPa and 5.7 and 30.5 MPa for a Ms = 1.4, respectively. While the SiMnS and LFS are less reactive resulting in AACs with flexural and compressive strengths of 3.2 and 11.6 MPa at Ms = 1.4 for SiMnS and 1.1 MPa and 4.6 MPa at Ms = 0.9 for LFS. In all AACs, the development of the alkaline activation reaction is confirmed due to the presence of gel, of different nature and quantity depending on the precursor used. The lower mechanical properties of the AACs using SiMnS and LFS as precursor may also be due to the presence of microcracks. Therefore, this study confirms that ferrous and non-ferrous slags can be used as precursors of AACs, with the type of precursor and the modulus of the activating solution influencing mechanical properties. AACs using CS and EAFS can be used in structural applications, while those using SiMnS and LFS can be used in non-structural applications in civil engineering.

1. Introduction

The main component of Portland cement is clinker, whose key reaction involved in its manufacture is the decomposition of calcium carbonate into calcium oxide and carbon dioxide (CO_2). This is why the production of Portland cement not only consumes a large amount of raw materials but also of energy, since clinkerization temperatures of 1450 °C are required. Therefore, the emission of a substantial amount of CO_2 and other greenhouse gases occurs both in the limestone calcination process and in the fuel combustion process. Total CO_2 emissions attributed to cement production contribute about 7 % of global CO_2 emissions (2.5 Gt/year) aggravating global warming and its consequences [1]. In order to achieve a more environmentally friendly and economically efficient cement industry, the search for new types of cement as alternative to current Portland cements is imperative. For this reason, both the major industries and the scientific community have directed their efforts in recent decades to the search for new innovative cement types [2]. During the last few years, cements with additions have been developed and commercialized with which the partial substitution of Porland cement (PC) has been achieved by incorporating chemically active materials, such as pozzolans, and industrial by-products such as ashes and steel slags [3] partially decreasing CO_2 emissions, but without achieving a significant reduction due to the fact that, as a general rule, large percentages of clinker are still used in the formulation. Currently, alkali activation cements or geopolymers are the most eco-efficient and promising green cements or hydraulic binders, due to their low environmental impact, therefore, they are materials that considerably reduce CO_2 emissions without compromising economic costs.

* Corresponding author. Department of Chemical, Environmental, and Materials Engineering, Higher Polytechnic School of Jaén, University of Jaén, Campus Las Lagunillas s/n, 23071, Jaén, Spain.
E-mail address: deliche@ujaen.es (D. Eliche Quesada).

https://doi.org/10.1016/j.cemconcomp.2023.105427
Received 17 January 2023; Received in revised form 23 December 2023; Accepted 28 December 2023
Available online 30 December 2023

Alkali-activation is a chemical reaction where a material rich in silicon and aluminum or calcium, silicon and aluminum, mixed with a solution of high alkalinity, forms a cementitious material [4]. In the current context of increasing resource scarcity and concern about climate change, the development of new sustainable building materials based on waste is vital. Which will have lower energy consumption during their manufacture and life cycle, lower CO_2 emissions to the atmosphere and improved properties.

The wide availability of metallurgical slags to avoid environmental damage [5,6], raises the question whether these wastes can be employed as precursors of alkaline activation materials providing part of the solution and becoming resources. Metallurgical slags can be divided into two main groups: ferrous slags and non-ferrous slags. Ferrous slags are those derived from iron and steel manufacturing processes, while non-ferrous slags are those derived from the manufacture of other metals. These last are produced on a smaller scale and they have a more variable and complex chemistry. Ferrous slags include blast furnace slags, electric arc furnace slags and ladle furnace or refining slags. Some 25.2 million tons of blast furnace slag and 22.6 million tons of electric arc furnace slag were produced in Europe in 2018 [7]. In Spain, the total steel production of the Spanish steel sector in 2018 was 14.3 million tons, 65.7 % being produced by electric arc furnaces, which translates into the production of 9.3 million tons of steel by electric way. Approximately, each tonne of steel produced generates around 130 kg of black slag and 25 kg of white slag, which would be equivalent to a black and white slag production of around 1,200,000 and 230,000 tons, respectively [8]. Most of the black slag is used in low value applications as aggregates in road construction, in the cement industry and as aggregate for concrete [9]. A small part, about 4 %, is destined for landfill mainly due to technical and legal impediments [8]. Therefore, there is a significant potential to recycle EAFS as a precursor in AAMs. The only alternative for industrial valorization of LFS is its use in cement factories as a substitute for marl, specifically in the manufacture of clinker [10]. Therefore, there is no technically and economically viable alternative use for this slag, and its most common destination is landfill disposal, causing serious problems in the short and medium term both for the generating companies and for the environment and society in general [11].

As for non-ferrous slag production, in 2016, refined copper production in the EU stood at 2.6 million tons, representing 12 % of global production. It should be noted that between 2 and 3 tons of copper slag are produced for each ton of copper manufactured, which notes the high generation of the waste [12,13]. In Spain in 2019, 623,043 tons of copper slags were produced [14]. The most important lines of research on copper slags for their use in civil engineering are mainly focused on the study of the behaviour of cements and concretes, and their pozzolanic properties. However, there are also alternative uses such as ballast for railroad lines, filler, granular layers for road surfaces, aggregates for the manufacture of bituminous mixtures, mortars and concretes, abrasives, addition to clinker, among other uses [15,16]. Regarding the generation of silico-manganese slag, between 0.9 and 2.2 tons of these slags are produced for each ton of silico-manganese ferroalloy manufactured [17]. In Spain, 162,086 tons of ferroalloy were produced in 2015, which confirms the high generation of the waste. The average utilization rate of these slags is 72 %, the rest being deposited in landfills [18]. The main applications of SiMnS are its use as an aggregate in pavement layers [19], as aggregate for concrete, as filler material in embankments, in addition to its use in railway applications [20].

The versatility of alkaline activation makes it suitable for the valorization of industrial by-products and wastes. The use of ferric slags, mainly blast furnace slags as precursors, has been widely studied. Thus, Wang et al. [21] investigated the effect of several factors (alkali activator type, alkali dosage, slag fineness, SiO_2/Na_2O ratio (modulus, Ms) when using sodium silicate solution, curing temperature, liquid/slag or water/slag ratio and additive) on the compressive strength of alkali activated ground granulated blast furnace slag (GGBS). Burciaga Díaz et al. [22], studied the chemical activation of blast furnace slag pastes with alkaline solutions, studying the microstructure as a function of the Ms modulus of the activator. In both studies, the optimum activation conditions of slags used were determined. The use of electric arc slags, ladle slags and non-ferrous slags as precursors for AAMs has been growing in interest in recent years. Thus, Ozturk et al. [23], studied the effect on mechanical and microstructural behaviour of different variables such as silicate modulus, sodium concentrations, curing conditions, curing temperatures and relative humidity conditions on alkali activation of electric arc furnace slag (EAFS) mortars. Experimental results revealed that increasing relative humidity, temperature and curing time have positive effects on strength due to decreased microcracking and altered hydration reactions. The authors conclude that EAFS can be successfully employed as a precursor for AAMs. Other authors have studied the use of EAFS waste in conjunction with other wastes. Thus, Apithanyasai et al. [24], investigated the relationship between concrete residue (CR) (100–60 wt %) and electric arc furnace slag (10–40 wt %) for the production of geopolymer bricks. As an alkaline solution sodium silicate (Na_2SiO_3) and sodium hydroxide (10 M NaOH) in a ratio of Na_2SiO_3 to 10 M NaOH of 2.5 was employed. The results showed that the incorporation of 20 wt% EAFS to CR was the optimum by yielding AAMs with the highest compressive strength value. Hafed et al. [25] studied the mechanical and durability properties of concrete activated with NaOH solution based on an electric arc furnace slag, fly-ash (FA) and EAFS (50 wt %)-FA (50 wt %). The results indicated that the compressive strength and durability decreases with the substitution of FA for EAFS as a precursor in the AACs mainly due to the lower amount of amorphous silica phases in EAFS.

Xu and Yi [26], studied the activation of ladle furnace slag (LFS) with sodium hydroxide (NaOH), sodium sulfate (Na_2SO_4), and sodium silicate (Na_2SiO_3), as well as, the use of mixed LFS: GGBS systems. The results indicated that LFS could not be effectively activated using these activators, obtaining compressive strengths of less than 2 MPa after 28 days of curing, while activation of the LFS-GGBS system produced a strength of up to 15.6 MPa. The results indicate that LFS-GGBS can be potentially used as a binding material in civil engineering. In another study, Adensanya et al. [27], studied the activation of LFS employing sodium silicate and potassium hydroxide as activating solution in different proportions to optimize the compressive strength of AACs, obtained values of 65 MPa after 28 days under the optimum conditions of silica and alkali metal contents. Thus, they conclude that the use of this highly crystalline slag as the sole precursor in alkaline activation is promising.

Kuterasinska and Krol [28], studied the alkaline activation of copper slags (CS) cured at 20 and 80 °C. The compressive strength of AAMs is significantly affected by the curing temperature, the amount and type of alkaline activator and the specific surface area of the CS. The best results are obtained for mortars employing sodium silicate, an activator modulus Ms = 1.75, high surface area and heat treatment. Nazer et al. [29], studied the alkaline activation of two copper slags collected from landfills. The AAMs were cured at different temperatures 20 and 65 °C. A solution of 5 M NaOH and sodium silicate, an activator modulus of 1.45 and a water/CS ratio of 0.25 were used as alkaline activator. The compressive strength of specimens cured for 3 days at 65 °C was like specimens cured for 90 days at 20 °C, obtaining values between 40 and 64 MPa. Qianmin et al. [30] researched the effect of NaOH concentration (6 M, 8 M, 10 M and 12 M) and high temperature exposure on the mechanical properties of alkali activated mortar based on copper slag. Strengths of the alkali activated mortars were very low at room temperature. However, after exposure to 200 °C, their strength increased dramatically due to the dissolution of some non-reactive CS particles at room temperature. Then, the strength of such a system started to decrease until the temperature increased to 800 °C where Fe_2O_3 could have melted filling the pores and cracks and making the matrix denser and stronger. Navarro et al. [31], investigated the hydration products obtained from alkaline activation of SiMn slag pastes using NaOH and

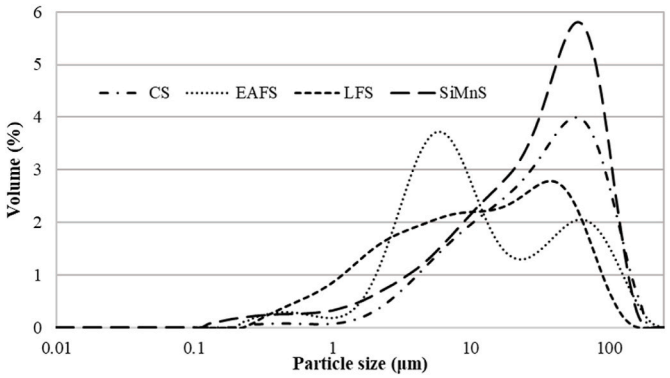

Fig. 1. Particle size distribution of ferrous slag: EAFS and LFS, and non-ferrous slags: CS and SiMnS.

waterglass with different Na_2O concentrations as activators. The results obtained indicate that the alkaline activation of SiMn slag gives rise to hydrated products and a microstructure similar to that obtained with other slags widely studied for the manufacture of alkaline activated cements, demonstrating the feasibility of valorizing the SiMn residue for this application. Kumara et al. [32], studied the use of SiMnS in the development of alkali activated cements. Slags were activated with a 6 M NaOH solution. The influence of the reactivity of the SiMnS by mechanical activation using different grinding devices such as the attrition mill and the eccentric vibratory mill was studied. The results indicate that mechanical activation increases the reactivity of SiMnS. Eccentric vibratory milling produced a more reactive SiMnS than attrition milling. In another study, Navarro et al. [33] researched the alkaline activation of SiMnS by studying the influence of $\%Na_2O$, the SiO_2/Na_2O ratio and the activating solution/slag ratio on different technological properties. The results show that workability decreases with increasing $\%Na_2O$ and decreasing SiO_2/Na_2O ratio. A compressive strength higher than 45 MPa can be achieved with the following activation conditions: 4.0–4.5% Na_2O, $SiO_2/Na_2O = 1.00$ and activating solution/slag = 0.35–0.375. In a previous study, Gómez-Casero et al. [34] investigated the influence of the molar concentration of KOH (5, 8, 12 and 15 M) on the alkaline activation of EAFS and CS using as activating solution a 1:3 ratio solution of KOH and K_2SiO_3. The results showed that optimum mechanical properties were obtained when 8 M M concentration of KOH was used for EAFS activation, while 8 M and 12 M concentrations of KOH were suitable for CS activation. In view of this background, the influence of the activator modulus (SiO_2/KOH) on the alkaline activation of EAFS and LFS ferrous slags and CS and SiMnS non-ferrous slags on the technological properties of alkaline activated cements has been studied.

2. Experimental program

2.1. Raw materials

In this investigation, different slags generated in ferrous and non-ferrous smelting processes are used for the synthesis of alkaline activated binders. Two slags from steel production in the electric arc furnace (Alcalá de Guadaira, Sevilla, Spain) were used: electric arc furnace slag (EAFS) (3–5 mm particle size) originated in the primary metallurgy or fusion and ladle furnace slag (LFS) (0–2 mm particle size) originated in the secondary metallurgy or refining of the molten bath produced in the ladle furnace. A slag from primary copper metallurgy, copper slag (CS), with 4 mm as maximum particle size, obtained in the pyrometallurgical process carried out by the smelting and refining company Atlantic Copper (Huelva, Spain). A slag from the production of silico-manganese, silico-manganese slag (SiMnS), with a maximum particle size of 20 mm produced in the electric arc furnace of the company Ferroatlántica (A Coruña, Spain).

EAFS, CS and SiMnS were first crushed in a hammer mill and then were crushed in a ball mill as LFS slags to ensure its reactivity and they were sieved through 0.1 mm sieve. A Malvern Mastersizer 2000 laser diffractometer was used to obtain the particle size distribution of slags. According to the particle size analysis, SiMnS and CS have a similar particle size distribution with $d_{50} = 35.40$ and 30.47 μm, respectively. LFS have a particle size distribution similar to non-ferrous slags but with a slightly lower average size $d_{50} = 11.35$ μm, while EAFS have a bimodal particle size distribution with a size $d_{50} = 8.68$ μm (Fig. 1).

X-ray fluorescence (XRF) is used to determine the chemical composition of slags (Table 1) determined with a Philips Magix Pro model PW-2440 equiment. As can be observed EAFS, LFS and SiMnS are mainly composed of CaO, SiO_2 and Al_2O_3, being EAFS rich in Fe_2O_3 (24.2 %), LFS in MgO (13.2 %) and SiMnS in MnO (9.53 %). EAFS and mainly LFS have high LOI values. CS are rich in Fe_2O_3 and SiO_2.

X-Ray Diffraction (XRD) was used to identify diffraction patterns of raw materials using a PANalytical Empyrean equipment with a PIXcel3D detector, while the identification phase was determined with HighScore software. A deviation from baseline was found in diffractogram of slags indicating a more amorphous structure. Wuestite (FeO), gehlenite ($Ca_2Al(SiAl)O_7$) and larnite (Ca_2SiO_4) were identified in EAFS. In the case of LFS, it presented peaks corresponding to calcio-olivine (Ca_2SiO_4), quartz (SiO_2) and brucite ($Mg(OH)_2$). Main diffraction peaks found in CS were fayalite ($(Fe^{2+})_2SiO_4$) and magnetite (Fe_3O_4). In SiMnS were identified peaks of quartz (SiO_2), akermanite ($Ca_2Mg(Si_2O_7)$) diopside ($MgCaSi_2O_6$) and alabandite (MnS) (Fig. 2).

It can be seen in the SEM micrographs of the ferrous slags show a wide particle size distribution with irregular, slightly rounded particles. In the SEM micrographs of the non-ferrous slags, a wide particle size distribution is also observed, with irregular angular and sharp particles. In the CS, larger particles are observed in accordance with the particle size distribution (Fig. 3).

2.2. Specimen preparation

Alkali activated cements (AACs) samples were prepared by mixing each of the ferrous and non-ferrous metallurgical slags used as precursor with the alkali activator. The alkali activator is classified according to the silicate modulus, Ms (mass ratio of SiO_2/K_2O). Four levels of silicate modulus were studied 0.5, 0.9, 1.4 and 1.8. For each Ms value, the wt. % of potassium silicate solution was set, and knowing these values, the quantity of KOH pellets, supplied by GlobalChem with 85 % of purity, necessary to obtain these ratios was determined. Total water for a concentration of KOH 8 M was made by taking the amount of water contained in the potassium silicate solution as part of the solvent. So that in addition to the water contained in the K_2SiO_3 solution, water had to be added to obtain the desired concentration (8 M). The solution was prepared by adding the calculated KOH pellets to distilled water, and then the calculated amount of potassium silicate was poured. The

Table 1
Specific gravity and chemical composition of raw materials: ferrous and non-ferrous slags.

	Specific gravity	SiO_2	Al_2O_3	Fe_2O_3	MnO	MgO	CaO	Na_2O	K_2O	SO_3	LOI	CaO/Si + Al
EAFS	3.24	17.29	10.71	24.16	5.68	2.63	30.89	0.16	0.03	0.28	5.39	1.10
LFS	2.81	22.26	8.32	6.75	1.34	13.2	33.24	0.53	0.64	1.85	10.76	1.09
CS	3.82	27.65	2.04	62.18	0.03	0.38	1.25	0.63	0.56	0.9	0	0.04
SiMnS	3.12	38.91	11.94	0.63	9.53	4.12	28.06	0.07	1.22	1.7	0	0.55

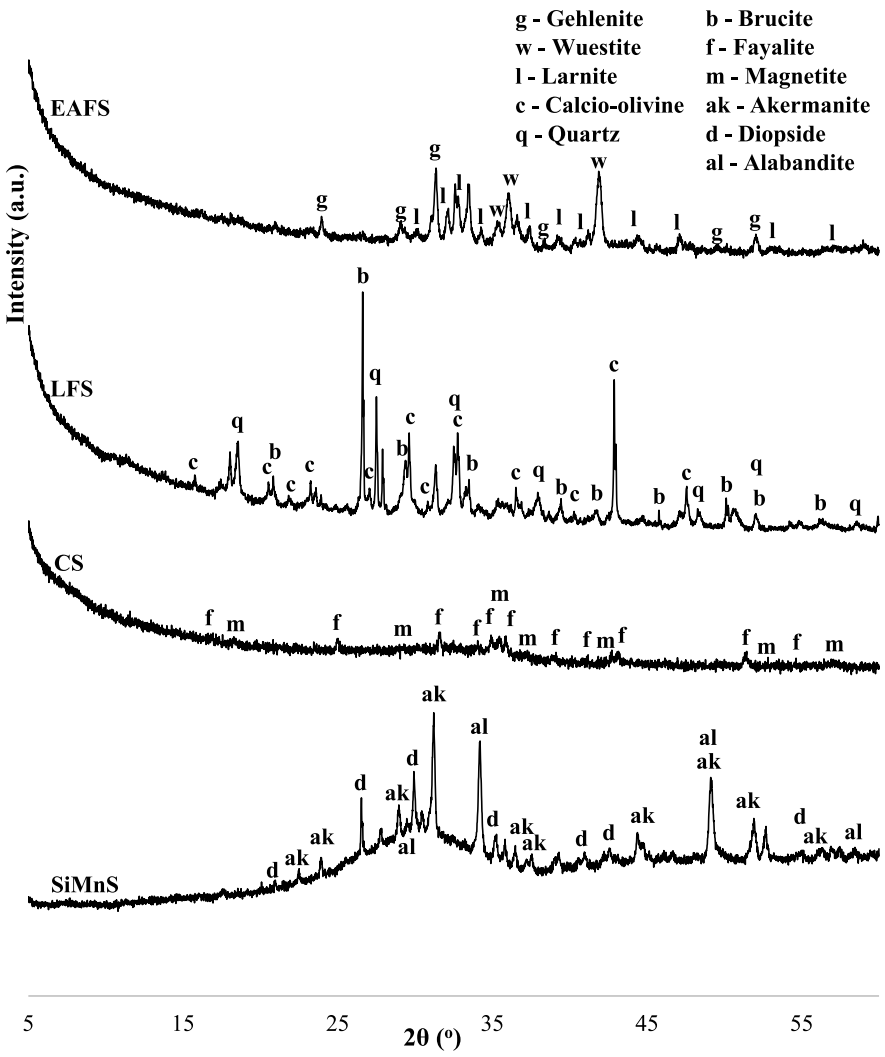

Fig. 2. XRD patterns of raw materials, ferrous and non-ferrous slags.

potassium silicate solution was supplied by Roth Company (7.5–8.7 % K_2O, 19.5–21.8 % SiO_2 and 69.5–73.0 % H_2O). Jansson et al. [35] reported that the silicate species in the activating solution consist of silicate monomer, attenuator, trimer and other higher order units. The increase in silicate modulus is more favorable to the presence of higher order silicate units. A constant liquid/binder ratio was used for each AACs employing the same precursor. The liquid/binder ratio for each type of slag has been modified in order to obtain the same workability of the paste. The liquid fraction includesKOH solution and potassium silicate solution. The workability was checked using the flow table test according to ASTM C-1437 [36], and results are shown in Table 2. It can be observed that all the pastes present values in the same range (168.0–204.5 %), which could indicate that they present similar workability. The unburned carbon content in EAFS but primarily in LFS slags reduces their reactive potential and contributes to the higher water demand of these blends. In addition, the residual carbon can behave as an alkali sink by adsorbing and effectively removing the alkali cations needed for the geopolymeric or alkaline activation reaction resulting in lower mechanical properties [37]. A summary of the AAC blend formulations is shown in Table 2. The AACs were designated by the precursor employed followed by silica modulus.

Precursors (each type of metallurgical slag) and the alkaline solution were mixed by planetary mixer for 90 s. Subsequently, a scrapper was used to stir the materials of walls and they were mixed for another 30 s. The paste was poured into a 10 × 10 × 60 mm steel prismatic mould. The fresh paste was subjected to 60 strokes on a vibrating table to remove air bubbles. The moulds were placed in a climatic chamber at 20 ± 1 °C and 90 % relative humidity for 1 day. Afterwards, the samples were demoulded and placed in the climatic chamber under the same conditions to continue curing until the age of tests 1, 7, 28 and 90 days.

A total of 24 samples with a nominal size of 10 × 10 × 60 mm were manufactured for each of the compositions. In addition, for the determination of thermal conductivity, two samples of 50 mm in diameter and 20 mm in height were manufactured.

2.3. Tests developed in AACs

Attenuated Total Reflectance Fourier Transform Infrared Spectroscopy (ATR-FTIR), using a Vertex 70 Bruker equipment in the range from 4000 to 400 cm^{-1} was used to characterize specimens. Crystalline phases formed were identified by XRD.

Mechanical strength (flexural and compressive strength) was determined following the standard UNE-EN 1015–11:2000/A1:2007 [38]. In the case of flexural strength, six prismatical samples of 10 × 10 × 60 mm nominal size were analyzed using a MTS Insight 5 machine (5 kN load capacity) and 0.2 mm/min displacement speed. One-half of the specimens tested was subjected to compressive strength using a universal testing machine MTS 8101 (100 KN load capacity) with 0.5 mm/min displacement speed. Some pieces of samples were selected to perform Scanning Electron Microscope (SEM) test using a JEOL SM 840 model.

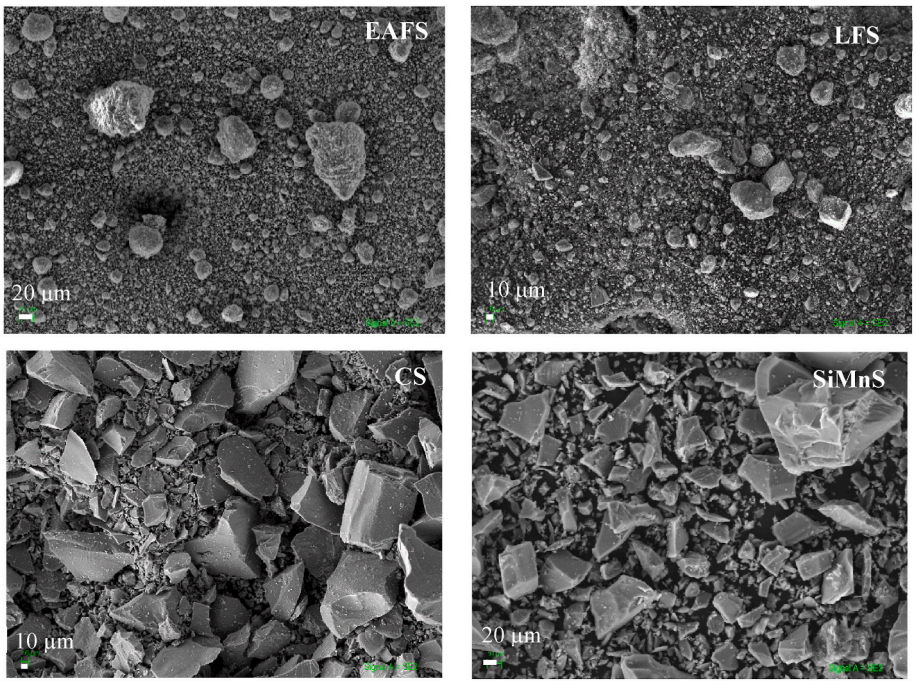

Fig. 3. SEM images of the precursors at 500*x*, EAFS and LFS ferrous slags and CS and SiMnS non-ferrous slags.

Table 2
AACs mix formulation and flow table test results.

Sample ID	EAFS (g)	LFS (g)	CS (g)	FS (g)	KH (g)	KSS (g)	Water in KSS (g)	Total water (g)	SiO_2/K_2O (Ms)	K_2O (%)	l/b	Flow (%) (ASTM C-1437)
EAFS-M0.5	400				53.91	84	59.9	161.9	0.5	65.26	0.60	177.2
EAFS-M0.9	400				41.47	120	85.5	164.0	0.9	52.98		173.7
EAFS-M1.4	400				29.03	156	111.2	166.1	1.4	41.93		168.0
EAFS-M1.8	400				20.73	180	128.3	167.5	1.8	35.16		172.2
LFS-M0.5		400			71.87	112	79.8	215.9	0.5	65.26	0.80	204.5
LFS-M0.9		400			55.29	160	114.0	218.7	0.9	52.98		184.8
LFS-M1.4		400			38.70	208	148.2	221.5	1.4	41.93		186.6
LFS-M1.8		400			27.64	240	171.0	223.4	1.8	35.16		188.9
CS-M0.5			400		31.45	49	34.9	94.5	0.5	65.26	0.35	201.5
CS-M0.9			400		24.19	70	49.9	95.7	0.9	52.98		200.9
CS-M1.4			400		16.93	91	64.8	96.9	1.4	41.93		194.2
CS-M1.8			400		12.09	105	74.8	97.7	1.8	35.16		195.4
SiMnS-M0.5				400	35.94	56	39.9	108.0	0.5	65.26	0.40	180.0
SiMnS-M0.9				400	27.64	80	57.0	109.4	0.9	52.98		195.1
SiMnS-M1.4				400	19.35	104	74.1	110.8	1.4	41.93		183.0
SiMnS-M1.8				400	13.82	120	85.5	111.4	1.8	35.16		187.0

KH: potassium hydroxide, KSS: potassium silicate solution; Ms: silica modulus. Water in KSS solution (71.25 %), total water: water in KSS solution plus water added to obtain a KOH 8 M, K_2O (%): % de K_2O in the activator, l/b: liquid to binder ratio. 'M0.5', 'M0.9' 'M1.4' or 'M1.8' behind precursor means the silica modulus of alkali solution to make AACs is 0.5, 0.9, 1.4 or 1.8.

The bulk density of the remaining halves of the specimens (six) subjected to flexural strength was obtained according to standard UNE-EN 1015–10 [39]. At 28 days of curing, a FOX 50 TA instruments heat flow was used to determine thermal conductivity of two cyclindrical samples (50 mm diameter, 20 mm height), according to ISO 8302 [40]. The equipment establishes steady state one-dimensional heat flux through a test specimen between two parallel plates at constant but different temperatures, 10 and 30 °C. Fourier's law of heat conduction is used to calculate thermal conductivity. By appropriate calibration of the heat flux transducers with calibration standards and by measurement of the plate temperatures and plate separation. Fourier's law of heat conduction is used to calculate the thermal conductivity. The experimental scheme followed in this study is shown in Fig. 4.

3. Results and discussion

3.1. Flexural and compressive strength

The strength of AACs is of great importance for their practical application and it depends on the chemical reaction between the precursor and the alkaline solution, as well as the reaction conditions, temperature and curing time [41]. In this study, the type of slag used as precursor, activator modulus (Ms) and curing age are considered as variables affecting the strength, with the curing temperature being room

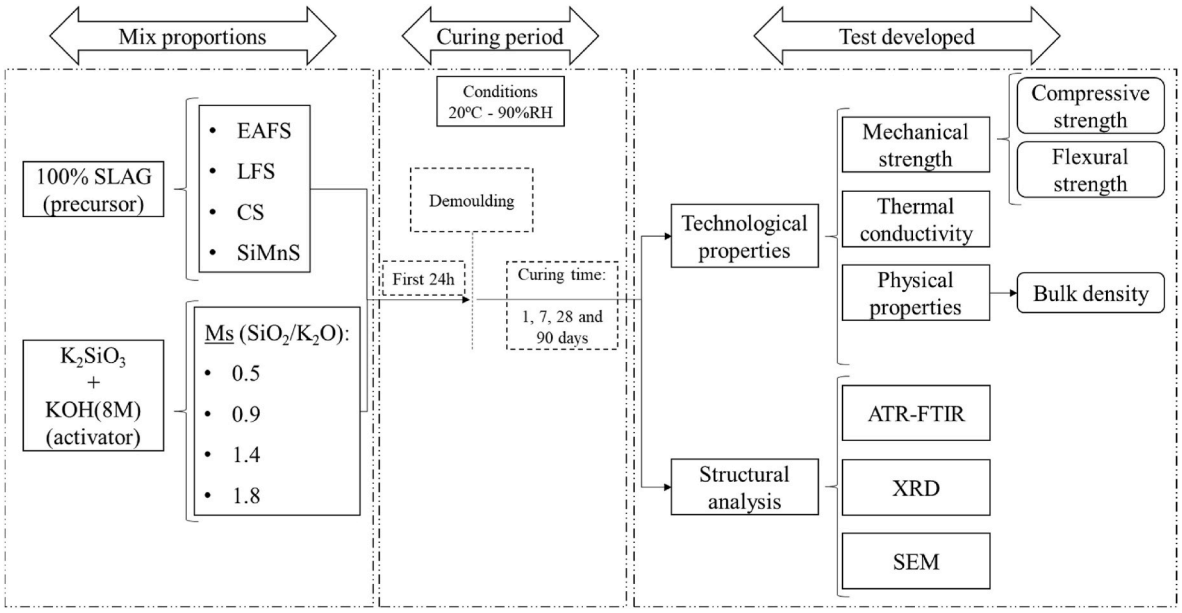

Fig. 4. Schematic of experimental procedure followed in this study.

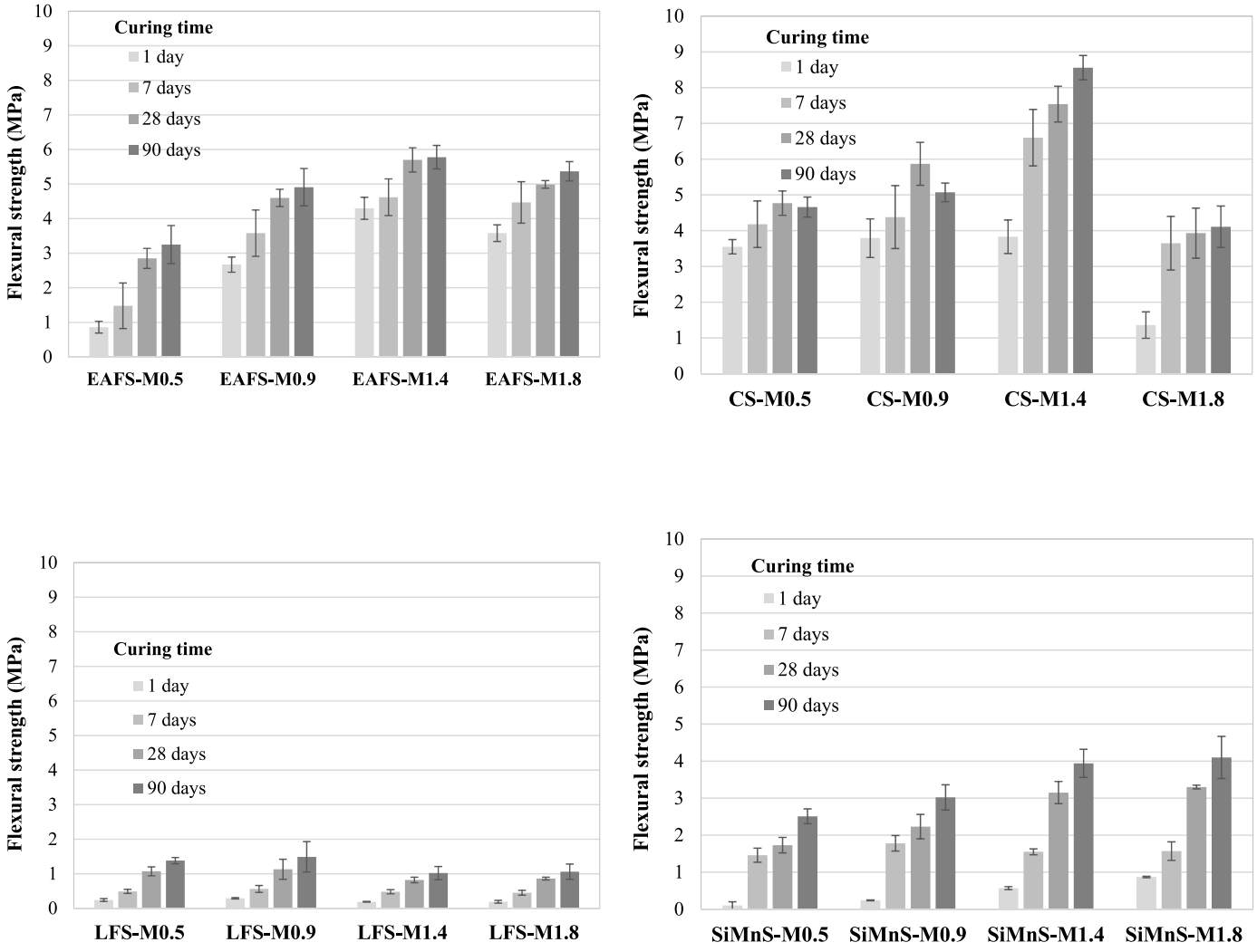

Fig. 5. Flexural strength of the different AACs as a function of the precursor, the modulus of the activator and the curing time.

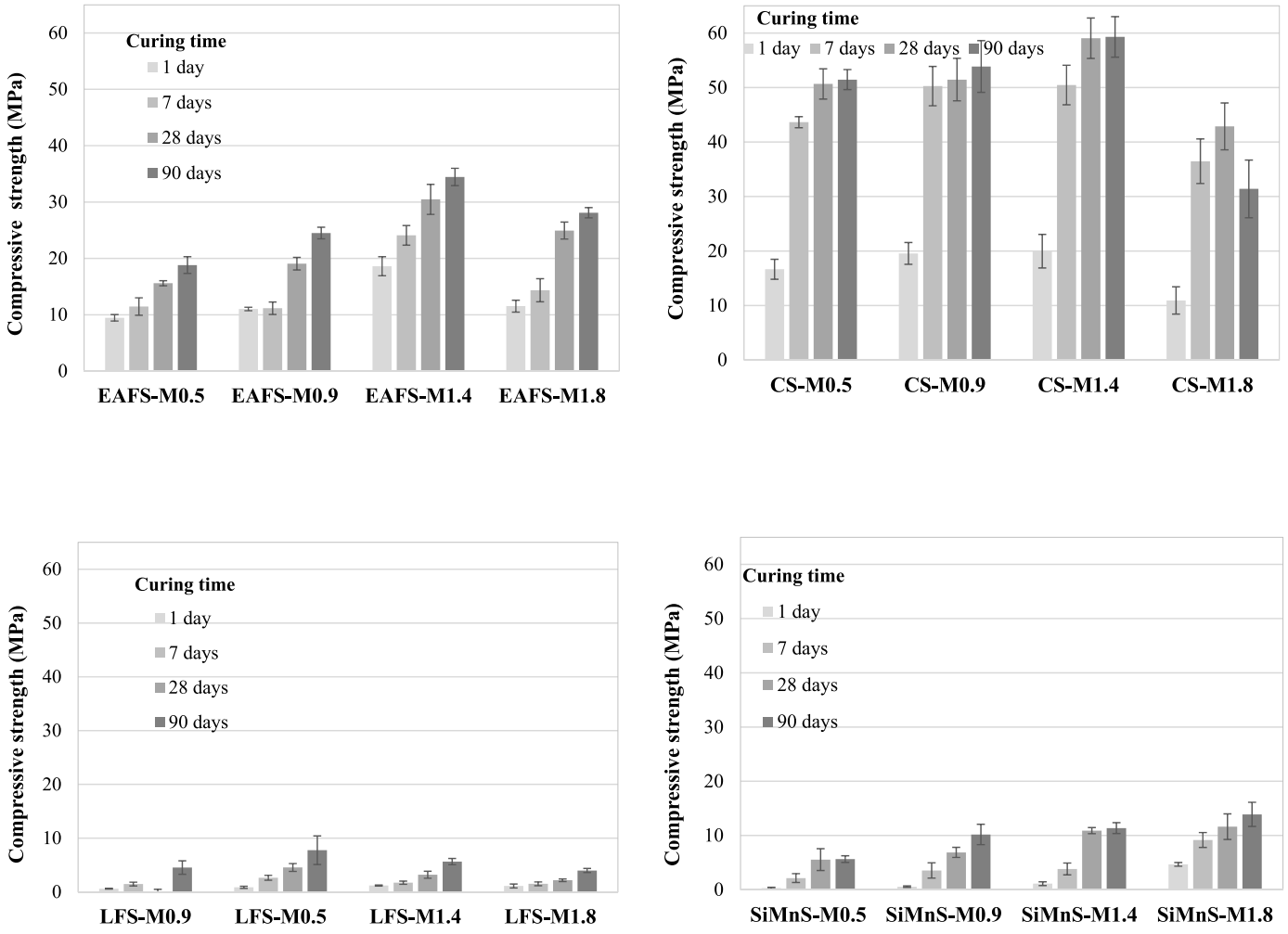

Fig. 6. Compressive strength of the different AACs as a function of the precursor, the modulus of the activator and the curing time.

temperature and relative humidity being 90 %. Figs. 5 and 6 shows the compressive strength and flexural strength of the different AACs as a function of the precursor used, the modulus of the activator used and the curing time. It can be observed that the flexural and compressive strength varies considerably as a function of the precursor used, the activator modulus and the curing time. Both strengths for AACs decrease with the type of precursor used: CS > EAFS > SiMnS > LFS and they depend on the chemical reaction between the precursor and the alkaline substances, as well as on the reaction conditions (activator modulus and curing time) [41] The different precursors have different reactive nature, which depends on the phase composition, proportion of crystalline and glassy phase, which is determined by the cooling conditions and the chemical composition [42]. Based on the CaO content presents in the chemical composition of the precursors, the products of the geopolymerization or alkaline activation process are divided into two main groups. Materials with low calcium content (Ca/(Si + Al) < 1) (CS and SiMnS slags) (Table 1) in which in the geopolymerization reaction an amorphous geopolymeric gel of hydrated potassium aluminosilicate (K-(A)-*S*-H) is formed after the phases of dissolution, condensation, reorganization, polycondensation, with or without crystallization, and finally solidification [43] and precursors containing large amounts of calcium (Ca/(Si + Al) > 1) (EAFS and LFS slags) (Table 1) that are activated with alkalis in a manner similar to the hydration of Portland cement forming hydrated calcium aluminosilicate gels (*C*-A-*S*-H). In addition, some by-products are formed in this reaction, such as the K-A-*S*-H gel [43,44]. The highest flexural strength and compression values are obtained for the AACs activated with the non-ferrous CS, and with the ferrous EAFS. The main elements of the CS are Fe_2O_3 (62.2 %) and SiO_2 (27.7 %) containing smaller amounts of Al_2O_3 (2.0 %) and CaO (1.3 %), precursor with low Ca content, while EAFS are CaO (30.9 %), Fe_2O_3 (24.2 %), SiO_2 (17.3 %) and Al_2O_3 (10.7 %) and in smaller amounts MnO (5.7 %) and MgO (2.6 %), precursor with high calcium content. The AACs using CS as precursor show maximum flexural and compressive strengths of 7.5 and 51.5 MPa after 28 days of curing when an activator modulus of Ms = 1.4 is used, increasing for a curing time of 90 days to 8.6 MPa and 59.3 MPa. The higher strength of the CS may be mainly due to the higher densification obtained in the AACs using this precursor (bulk density between 2600 and 2800 kg/m^3) and to a lesser extent to the higher reactivity due to the presence of amorphous material. In the alkaline medium not only the Si and Al present in the CS dissolve forming geopolymeric gel or hydrated potassium aluminosilicate gel (K-(A)-*Si*-H) but also the Fe present dissolves and forms Fe silicate complexes or other soluble complexes that prevent the immediate precipitation of Fe hydroxides, contributing to the formation of the binder [45]. Fe^{3+} ions, can substitute for aluminum in many compounds, due to their similar ionic radius and charge, and behave similarly during various chemical reactions [46]. The presence of aluminium in AACs accelerates condensation reactions, resulting in higher compressive strength and faster setting [47]. Therefore, the oxidation of Fe^{2+} present in the amorphous fraction of slags [48,49] to Fe^{3+} can also control the kinetics of condensation reactions in AACs, and Fe^{3+} contributes to the strength and setting behaviour of Fe-rich AACs [50]. The optimum flexural strength and compressive strengths of the AACs using EAFS as precursor are 5.7 and 30.5 MPa for a cure time of 28 days and

Ms = 1.4, with the flexural strength practically maintaining 5.8 MPa and the compression strength slightly increasing to 34.5 MPa after 90 days of curing. These AACs have bulk densities of 1750–1850 kg/m^3, much lower than the bulk densities of AACs using CS as precursor, so the mechanical strength is probably due to the amount of amorphous or reactive phase in these slags. As well as the introduction of soluble Ca^{2+} ions favors the formation of hydrated calcium aluminosilicate gel (*C*-(A)-*S*-H) that acts as nucleation sites and promotes rapid geopolymerization and the formation of a geopolymeric gel (K-A-*S*-H) to a lesser extent [51,52] forming an increased amount of reaction products occupying the pore space resulting in increased flexural and compressive strength [53,54]. As in CS, Fe dissolves in the alkaline solution and it is incorporated into the binder phase. When SiMnS with chemical composition rich in SiO_2 (38.9 %), CaO (28.1 %), Al_2O_3 (11.9 %), MnO (9.5 %) and to a lesser extent MgO (4.1 %) and LFS rich in CaO (33.2 %), SiO_2 (22.3 %), MgO (13.2 %), Al_2O_3 (8.32 %) and Fe_2O_3 (6.8 %) were used as precursors lower flexural and compressive strengths were obtained. For the AACs using SiMnS, maximum flexural and compressive strengths of 3.2 and 11.6 MPa were obtained for a curing time of 28 days and Ms = 1.8, increasing to 4.1 MPa and 13.9 MPa after 90 days of curing. However, for the AACs using LFS, lower values with flexural strength of 1.1 MPa and compressive strength of 4.6 MPa for a cure time of 28 days and a Ms = 0.9, increasing to 1.5 and 7.8 MPa, respectively, when the cure time is increased to 90 days. These data indicate that under the activation conditions used SiMnS and LFS are weaker pozzolans that develop lower mechanical strengths. The low flexural and compressive strength of AACs using LFS slags as precursor may be due to the high crystallinity of the precursor giving under the activation conditions used in the geopolymerization process a small dissolution of reactive species, Si and Al, leading to the formation of small amounts of K-A-*S*-H gel. Since these slags present a high amount of CaO, the dissolved Ca^{2+} ions can react with the *Si*–*O*–Si or Al–*O*–Si bonds and also form small amounts of *C*-A-*S*-H gel or hybrid (C,K)-A-S.H gel. In addition, their high free lime (CaO) and free magnesia (MgO) content [55] makes them susceptible to strength and expansion problems when it is hydrated. Unlike free lime, free magnesia usually hydrates at a slower rate and causes volumetric expansion over an extended period of time, i.e., months or even years [56]. Therefore, the appearance of microcracks due to expansion reactions leads to a decrease in the flexural strength and compression set of AACs using LFS as precursor. The low mechanical strengths obtained for SiMnS cements may be due to lower gel formation, as well as to the occurrence of fracture microcracks generated by both material shrinkage and water evaporation [57]. At higher Ms a more hydrophobic gel is formed which gives rise to expansive reactions and generation of microcracks as indicated by SEM analysis.

The curing time also has an effect on the flexural and compression strength of the AACs. It can be observed that the highest values of both strengths of the AACs, independent of the precursor and the modulus of the Ms activator used, are obtained after 90 days of curing indicating a continuation of the alkaline activation or geopolymerization reactions with time. However, it is observed that AACs using CS have a great growth of flexural strength and compressive strength the first 7 days of curing, with less growth up to 28 and 90 days of curing. In ACCs using EAFS as precursor, after 1 day of curing, flexural strength values between 0.9–4.6 MPa and compressive strength between 9.5 and 18.6 MPa, with flexural strength values increasing up to 3.3 and 5.8 MPa and compressive strength increasing more linearly with curing time up to 18.8–34.5 MPa after 90 days of curing. The high calcium content in the EAFS residue, due to its easy dissolution, is responsible for the rapid increase in compressive strength at early curing ages [58]. For the less reactive SiMnS and LFS the curing time produces a significant increase in flexural and compressive strength due to the slower dissolution rate. The AACs using SiMnS show flexural strength of 0.1–0.9 MPa and compressive strength between 0.3 and 4.7 MPa after 1 day of curing. However, the flexural and compressive strength values suffer a remarkable increase with values up to 2.5–4.1 MPa for flexural strength and 5.7–13.9 MPa for compressive strength after 90 days of curing. The AACs using LFS as precursor, a weak pozzolan that develops low early strength obtaining flexural strength values below 0.5 MPa and compressive strength values below 1.2 MPa after 1 day of curing with activation conditions used. The increase in flexural strength improves slightly with curing time and after 90 days of curing reaches flexural strength values between 1.1 and 1.5 MPa and compressive strength values between 4.0 and 7.8 MPa. The slow pozzolanic reaction allows all the AACs to develop higher flexural and compression strengths in the long term, however, high values are not achieved, due to the expansion that causes microcracks developed, as indicated above.

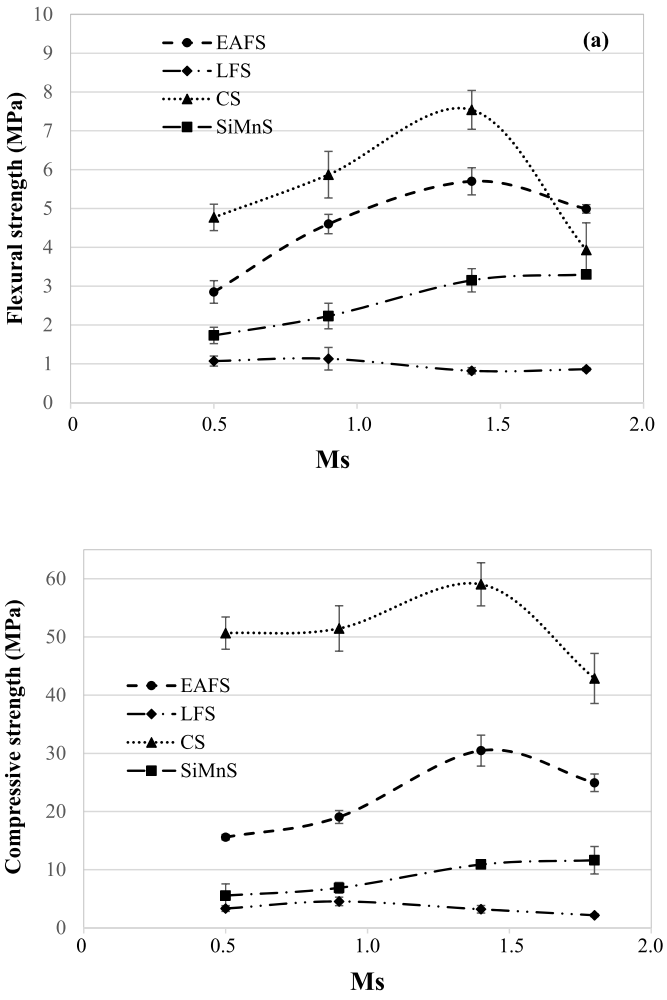

Fig. 7. (a) Flexural strength and (b) compressive strength of the different AACs as a function of activator modulus for each precursor used for a 28-day cure time.

Fig. 7 shows the flexural and compressive strength of the different AACs as a function of activator modulus for each precursor used at 28 days of curing. It can be seen that the flexural and compressive strength depend not only on the reactivity of different slags but also on the ability of the alkaline solution to leach reactive elements into the reaction medium [59]. Flexural and compressive strength gradually increased with increasing Ms values from 0.5 to 1.4 for AACs employing CS and EAFS, producing a further increase in Ms up to 1.8 a decrease in compressive strength. For AACs using LFS waste as precursor, an increase up to Ms 0.9 is observed, producing a decrease in mechanical properties when Ms of 1.4 and 1.8 are used, while for AACs using SiMnS, optimum values are obtained for a Ms of 1.8. Therefore, for each type of slag there is an optimum amount of soluble silicate which, if exceeded or not reached, significantly affects the mechanical properties of the alkali

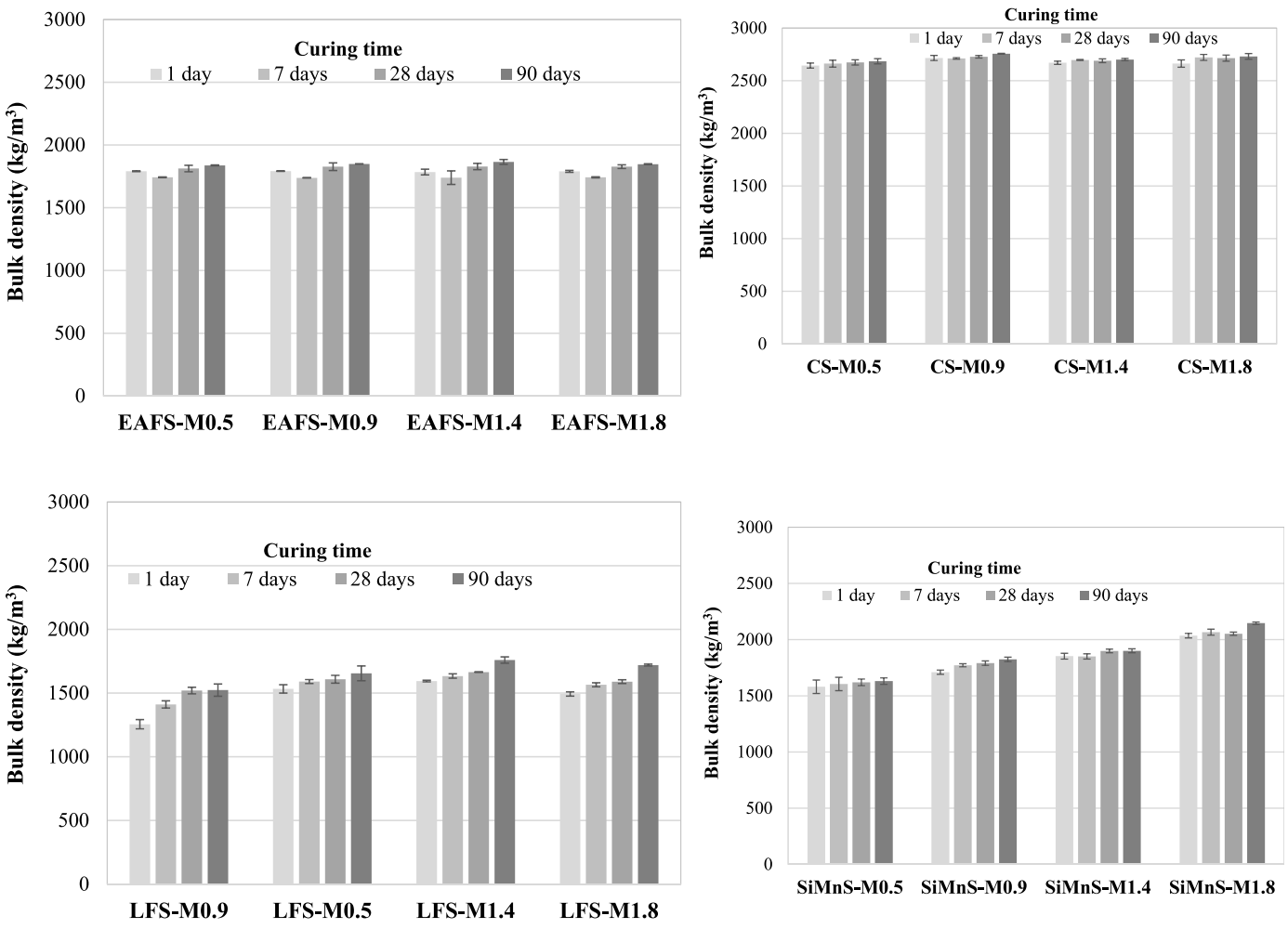

Fig. 8. Bulk density of the AACs as function of precursor, activator module and curing time.

activated cement. A defect (Ms = 0.5) such as an excess of sodium silicate in the activator (Ms = 1.5 for LSF cements, Ms = 1.8 for EASF and CS cements, and Ms > 1.8 for SiMnS cements) results in the geopolymeric structures formed not being the most suitable and not having the best physicochemical properties. The addition of optimum amounts of silicate species leads to an increase in the concentrations of soluble Si ions of the potassium silicate agent resulting in enhanced condensation which induces greater geopolymerization of the silicate units due to the additional silicate anions in the activating solution at higher Ms [60–62]. The higher silicate content results in longer Si chains leading to denser gels with superior mechanical strength [60]. Therefore, potassium silicate solution enhances the dissolution rate of Si, Al, Ca, and Fe, which come from precursors, as Al, Ca, and Fe dissolve faster than Si [63]. If Si ion is provided before it is available in the precursor through dissolution, it can increase the degree of geopolymerization producing more K-(Fe)-(A)-*S*-H and *C*-(Fe)-(A)-*S*-H gels [64]. An excessive activator module content, activator modulus Ms = 1.8, except for AACs employing SiMnS as precursor, due to an excess of silicate ions from the alkali solution which hydrate together with Al^{3+}, Ca^{2+} and Fe^{3+} ions and precipitate rapidly on the slag grains inhibiting the dissolution of the slag grains, inhibiting the alkali activation reactions, resulting in insufficient amounts of gel, making the behaviors less resistant [67,68]. Therefore, a high activator modulus results in a more viscous alkaline activator solution, reducing the workability of the paste and setting time [65,66], whereby, reaction products are rapidly formed in the highly alkaline medium inhibiting the geopolymerization reaction. While a lower activator modulus Ms = 0.5 results in less dissolution of ions present in the slag leading to less gel formation [68,69]. Excess OH^- accelerates polycondensation reactions leading to incomplete dissolution of aluminosilicates, causing early precipitation of the hydration gel, resulting in binders with low strengths because of an immature molecular structure. Excess Na^+ remaining unreacted in the matrix can lead to efflorescence formation due to the accumulation of carbonated sodium oxide on the cement surface [70]. Singh and Singh [71]. obtained compressive strengths of 34.1 MPa after 28 days of curing using CS with a 7 % alkaline activator solution of sodium hydroxide and sodium silicate (Ms = 1.25) and water/solid ratio of 0.3. Specimens were cured at 80 °C (24 h) and subsequently at room temperature. Kuterasińska and Król [28], obtained maximum compressive strength after 28 days of curing employing sodium hydroxide and sodium silicate as activator (Ms = 1.75) and CS as precursor. The maxium obtained was 21.0 MPa after 28 days of curing at room temperature, increasing up to 60 MPa with heat curing at 90 °C for 6 h and then at room temperature. Ameri et al. [72] obtained flexural strength of 5.7 and compressive strength of 59.2 MPa after 28 days of curing when CS was used as precursor and a solution of sodium silicate and sodium hydroxide in a mass ratio of 40.7–59.3 % as activator, and binder cured at room temperature. The maximum flexural strength and compressive values obtained in this study with the CS precursor after 28 days of curing are 7.5 and 51.5 MPa, respectively, using an activator modulus of 1.4. Therefore, the values obtained are higher than those obtained by other authors when they are cured at room temperature, being slightly lower than those obtained by heat treatment.

Ozturk et al. [73] indicated that in order to maximize the flexural

and compressive strength values of geopolymer mortars using EAFS as a precursor and sodium hydroxide and sodium silicate as activator solution, silica modulus, sodium concentration and curing conditions such as time, temperature and relative humidity of 1.4, 7.3 %, 98 %, 80 °C and 12 h, respectively. They obtained values of 3.38 and 18.65 MPa of flexural and compressive strength respectively. Nikolić et al. [74], compressive strength values of 21.04 MPa were obtained using EAFS as precursor using as alkaline activator in a mass ratio of 4:1, a Na_2SiO_3 solution, prepared by mixing 10 M NaOH and commercial sodium silicate. Curing took place for 2 days at 65 °C and then at room temperature for up to 28 days. In this work, when EAFS is used as a precursor, higher flexural and compressive strengths are obtained after 28 days of curing, 5.7 MPa and 30.5 MPa, respectively, when an activator modulus of 1.4 was used. In addition, the specimens are cured at ambient temperature with technical and economic advantages.

Su et al. [75], activated SiMnS with waterglass and NaOH with different activator modulus (Ms) between 0.9 and 2.1. Samples were cured at 60 °C until the age of the test (1 h–24 h) obtaining compressive strength values of 66.5 MPa at 24 h of curing. The high curing temperature was an important factor for its high mechanical behaviour in compression. Kumara et al. [76], activated SiMnS by altering the reactivity by mechanical activation with a 6 M NaOH activating solution. Compressive strength values ranging from 24 MPa were obtained for ball mill activation to 101 MPa when activated by vibratory milling. The values obtained in this study are lower, obtaining a compressive strength after 28 days of curing of 11.6 MPa using a Ms = 1.8. However, slags have not been mechanically activated and the curing has been carried out at room temperature.

Adesanya et al. (2017) [77] activated LFS with Na_2SiO_3 and KOH obtaining AACs cured at 60° (24 h) with an optimum compressive strength of 65 MPa after 28 days of curing. In contrast, Xu and Yi [78] obtained compressive strengths below 2 MPa after 28 days of curing at room temperature by activation with sodium hydroxide (4 M) and sodium silicate of LFS. Shi [54] also obtained a compressive strength of 10 MPa at 28 days of curing for Na_2SiO_3-activated LFS mortars. Wanga et al. [79] used LFS as precursor activated with a fixed alkali modulus ratio (SiO_2/Na_2O) of 1. Different liquid/solid (l/s) ratios of 0.35, 0.40 and 0.45 and alkaline agent amount of 4 %, 6 % and 8 % were studied. Curing was performed under different conditions (air and saturated lime water). The results indicate that when the curing is carried out at room temperature, maximum compressive strengths of 9 and 8 MPa are obtained after 7 and 28 days of curing respectively, using a l/s ratio of 0.35 and 8 % alkaline agent. These contradictory results could be due to the large variation of LFS properties. In this study, the maximum flexural strength values were 1.5 MPa and compressive strength 7.8 MPa for an activator modulus of 0.9 and 90 days of curing. Mechanical strength results indicate that while activation using KOH and K_2SiO_3 of CS and EAFS is effective, activation of LFS and SiMnS is not effective in achieving flexural and compressive strength suitable for civil engineering applications. In view of the results in the literature, additional activation by thermal curing or mechanical activation would be necessary.

3.2. Bulk density

The bulk density of ACCs depends on the amount of unreacted precursor, the mesoporous nature of the gel formed and the entrapped air. Fig. 8 shows the bulk density of the AACs as a function of the type of precursor used, the curing time and the activator modulus. It can be observed that the type of precursor has great influence on the bulk density. The bulk density values follow the decreasing order CS > SiMnS > EAFS > LFS according to the real density data of the precursors CS = 3832 kg/m^3, EAFS = 3245 kg/m^3, SiMnS = 3123 kg/m^3 and LFA = 2861 kg/m^3 (Table 1). Using CS as precursor was obtained the densest AACs with bulk densities between 2662 and 2721 kg/m^3 after 28 days of curing. EAFS and SiMnS activated AACs show the most similar bulk

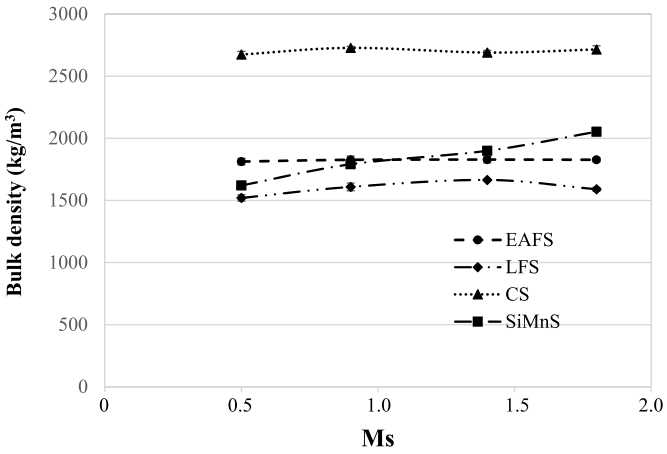

Fig. 9. Bulk density of the different AACs as function of activator module for a curing time of 28 days.

density values between 1812 and 1830 kg/m^3 and 1600–2052 kg/m^3, respectively for 28 days of curing. AACs based on LFS present the lowest bulk density values between 1519 and 1664 kg/m^3 at same curing time in accordance with the lowest real density of the LFS precursor. In addition, the l/b ratio (Table 2) to achieve an adequate consistency of pastes is different. In pastes using higher l/b (LFS and EAFS), higher porosity can be formed as a consequence of the elimination of excess water in the mixture that escapes to the environment during the curing process which will induce pores in the matrix of the alkaline activated materials, resulting in lower bulk density values. Increased liquid content (low b/l ratio) resulted in higher porosity values.

As for the influence of curing time, an increase in bulk density is observed when the curing time increases from 1 to 90 days, except in AACs using EAFS as precursor where for a curing time of 1–7 days the bulk density is reduced, due to the release of excess water, after which the density increases slightly. The loss of moisture during the curing process indicates an advance of the geopolymerization or alkaline activation reactions resulting in a greater amount of more compact gel that reduces the porosity.

As for the influence of the modulus of the activator (Fig. 9) for 28 days of curing, it can be observed that the trend is different in the reaction conditions studied. The same trend being observed for the AACs manufactured with precursors more reactive, CS and EAFS, as well as, for less reactive precursors, SiMnS and LFS. In the latter, the influence of the silica modulus is more notable, with more significant variations in bulk density being observed as a function of the Ms employed. The maximum bulk densities of the AACs using less reactive precursors are obtained for a Ms = 1.8 using SiMnS and Ms = 0.9 for LFS, due to the higher dissolution of the active phases of the precursor resulting in an increase of the geopolymerization reaction and the reduction of the porosity in the matrix [80], according to the mechanical strength data. Therefore, for the less reactive precursors, SiMnS and LFS, when non-optimal Ms values are used there is a higher amount of unreacted materials in the specimens, resulting in less gel formation by a slow activation process in the early stages due to high alkali content for small Ms and less matrix densification [61]. In the case of AACs using the most reactive precursors, the silica modulus, Ms, appears to have virtually no effect on bulk density at any cure time, with no significant difference found. Using a high Ms, there is a greater amount of potassium silicate which increases the viscosity of the alkaline solution, contributing to the compactness of the structure, but the activation process can be slow at early ages due to low alkali content [81]. However, when a low Ms is used, the geopolymerization process in the early stages can be rapid, forming gel particles that can envelop unreacted slag particles and partially prevent them from undergoing the activation reaction [82]. These unreacted particles can bind together acting as a filler, increasing

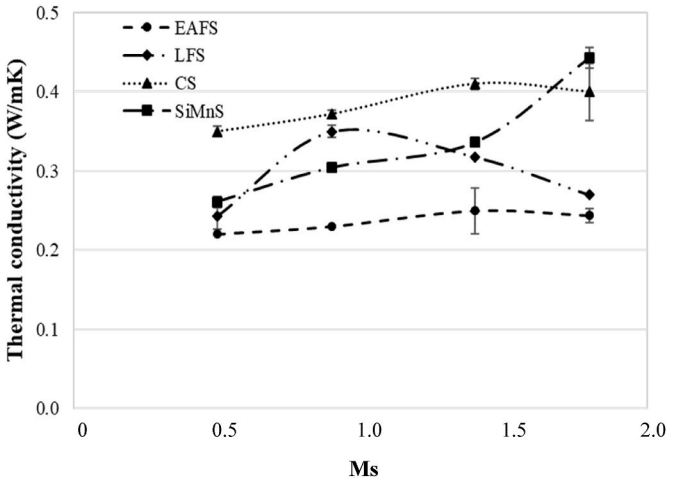

Fig. 10. Themal conductity of the AACs as function of precursor, activator module for a curing time of 28 days.

the density of specimens. Therefore, no relationship between bulk density and compressive strength is found for these AACs.

3.3. Thermal conductivity

Fig. 10 shows the thermal conductivity of the specimens after 28 days of curing. It can be observed that the thermal conductivity depends on the precursor used in the manufacture of the AACs, and there is no correlation between the bulk density of the specimens and the thermal conductivity. The thermal conductivity of the air, present in the voids, is lower than the conductivity of solid substances. However, the amount and composition of solid substances formed in AACs using slags of different nature, as well as, the amount of unreacted slag particles having different intrinsic thermal properties, can lead to different thermal conductivities. Regarding the influence of Ms, the same trend is observed as in bulk density, while the AACs using the most reactive slags, non-ferrous slag, CS, and ferrous slag, EAFS, show smaller variations in thermal conductivity data with values between 0.35 and 0.41 W/mK and 0.22–0.25 W/mK, respectively. Binders using less reactive slags, non-ferrous slag, SiMnS, and ferrous slag, LFS, show a higher variation in thermal conductivity data with values between 0.26 and 0.44 W/mK and 0.24–0.35 W/mK. It is observed that higher thermal conductivity values are obtained for the optimum Ms in the AACs. This is due, as previously mentioned, to the acceleration of the polycondensation and solification reactions, resulting in a greater amount of

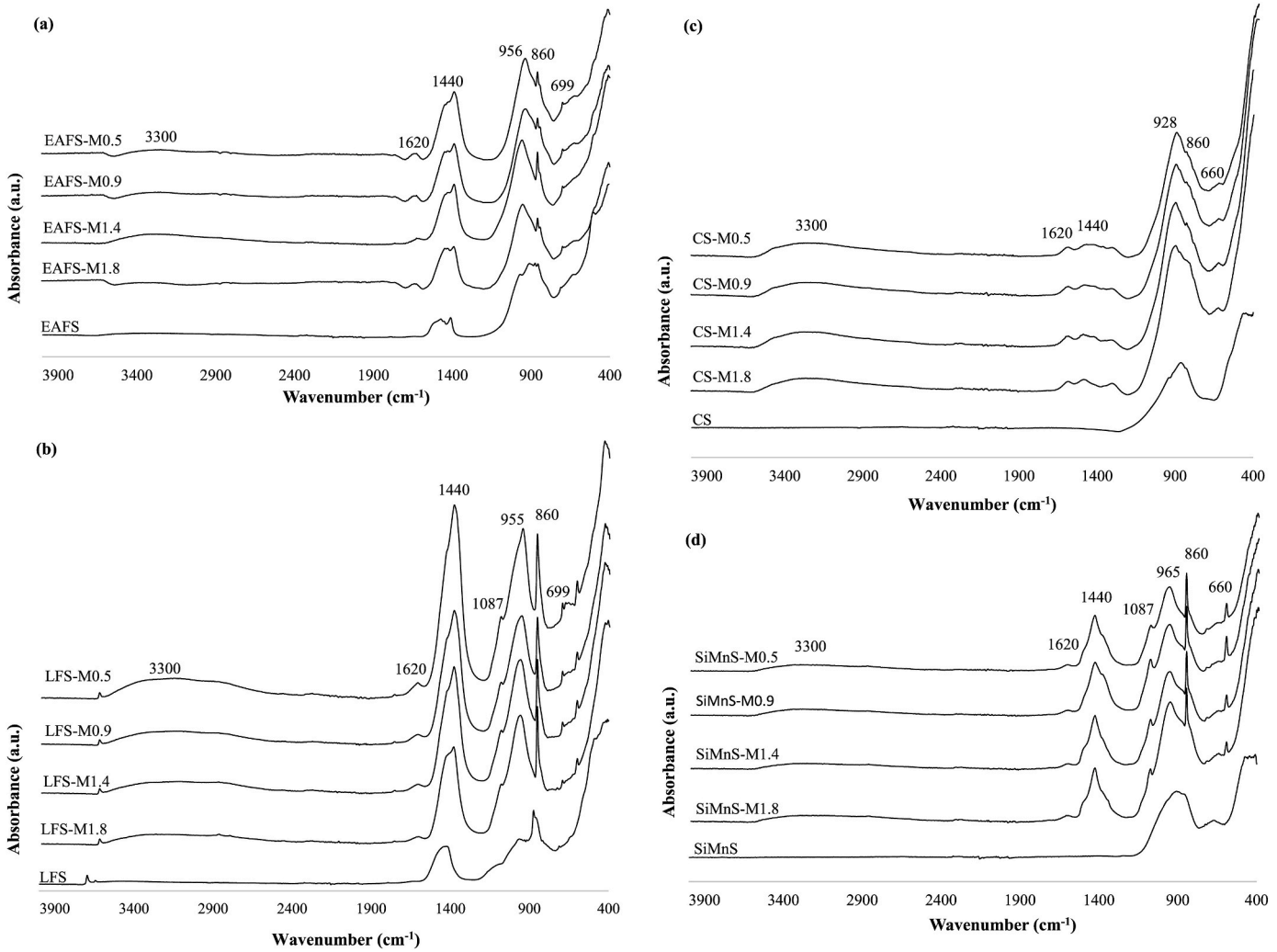

Fig. 11. FTIR spectra of the AACs as function of activator module for a curing time of 28 days. (a) EAFS cements and precursor; (b) LFS cements and precursor; (c) CS cements and precursor and (d) SiMnS cements and precursor.

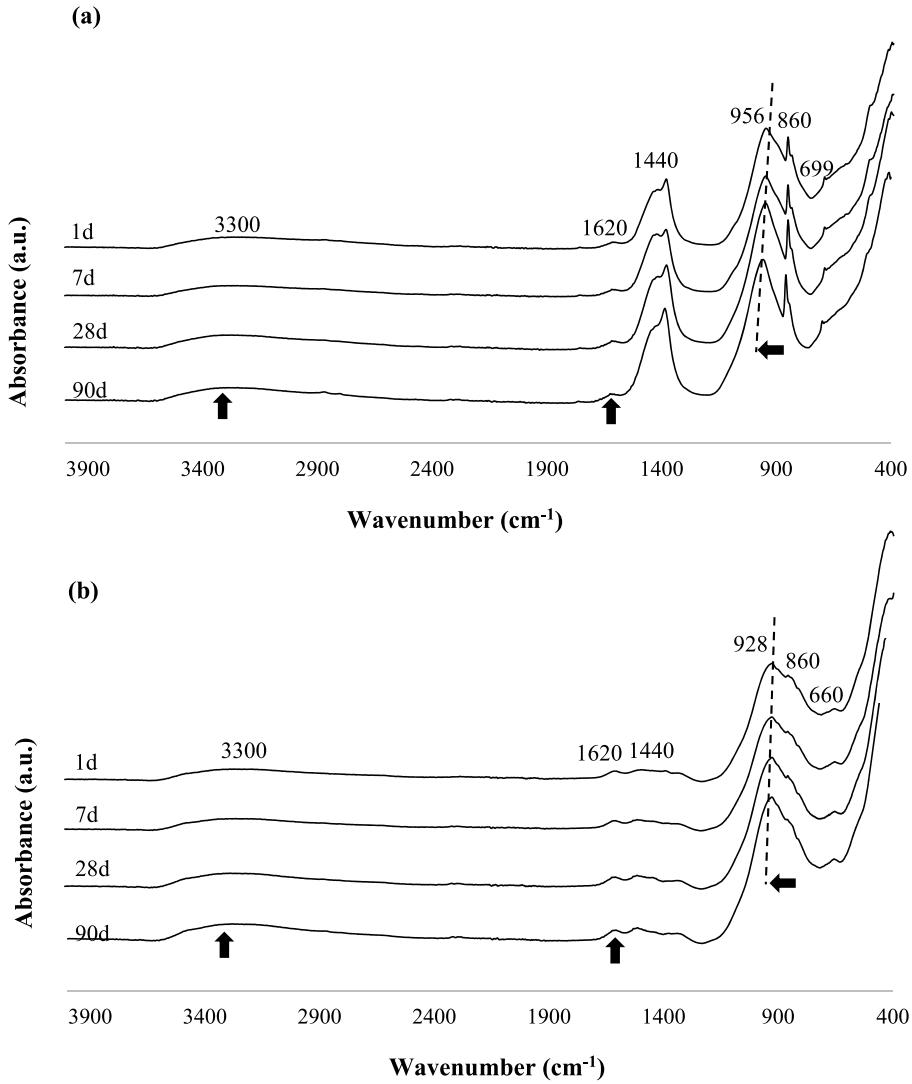

Fig. 12. FTIR spectra of the AACs af function of curing time (a) EAFS cements and (b) CS cements.

gel, making the internal structure more compact and giving rise to a lower thermal insulation capacity.

3.4. FTIR

The FTIR spectra of the alkaline activated binders using different slags as precursors as a function of the modulus of the activator for 28 days of curing are shown in Fig. 11. The FTIR spectra of precursors have been incorporated for comparison.

It can be observed in all the FTIR spectra regardless of the precursor used the presence of new bands centered around 3300 cm^{-1} and 1620 cm^{-1} attributed to the presence of OH groups related to the hydration products. The former attributed to the asymmetric and symmetric stretching vibrations of the *O*–H bond and the latter to the bending vibrations of the H–*O*–H bond [83,84]. The bands centered at 1440 cm^{-1} and 860 cm^{-1} can be attributed to the deformation and bending vibration of the *O*–*C*–O bond in carbonates, respectively, indicating the formation of carbonate products, as a consequence of the interaction of alkaline hydroxide with air [85,86]. Spectra of alkaline activated materials using steel slags, EAFS and LFS, show bands centered at 699 cm^{-1} attributed to the asymmetric bending vibrations of the *Si*–O bond, while these bands are shifted to 660 cm^{-1} for alkali activated cements using non-ferrous slags, CS and SiMnS [87]. In the spectra of AACs employing EAFS and CS, with iron-rich precursors, a very broad band centered at 956 cm^{-1} and 928 cm^{-1}, respectively, is observed, while in AACs employing LFS and SiMnS, in addition to the band centered at approximately 955 and 965 cm^{-1}, respectively, a peak centered at approximately 1087 cm^{-1} is observed. This broad band corresponds to the symmetric *Si*–*O*-T stretching vibration, (T = Si or Al) which was induced by K-(A)-*S*-H and *C*-(A)-*S*-H gel formation during alkaline activation of ferrous and non-ferrous slags [88–90]. In addition, the Fe present mainly in CS and EAFS slags is partially oxidized to Fe^{3+} after activation which can be incorporated into the silicate network changing the *Si*–*O*–Si into *Si*–*O*–Fe [91]. It can be observed that this band shifts to lower wavenumbers with respect to the precursors. This shift to lower wavenumbers could indicate a higher degree of silicate polymerization or a higher amount of gel produced by the hydration reaction, which isin agreement with the compressive strength results.

Regarding the influence of the curing time from 1 to 90 days (Fig. 12), a slight increase of the bands centered at 3300 cm^{-1} and 1620 cm^{-1} can be observed, due to a further advancement of the hydration reaction. Water is an important factor in the geopolymerization process, as it helps in the separation and hydrolysis of solid particles to form dissolved cations [92]. In addition, a slight shift towards higher frequencies of the T-O stretching band is observed, indicating slightly higher gel formation with curing time.

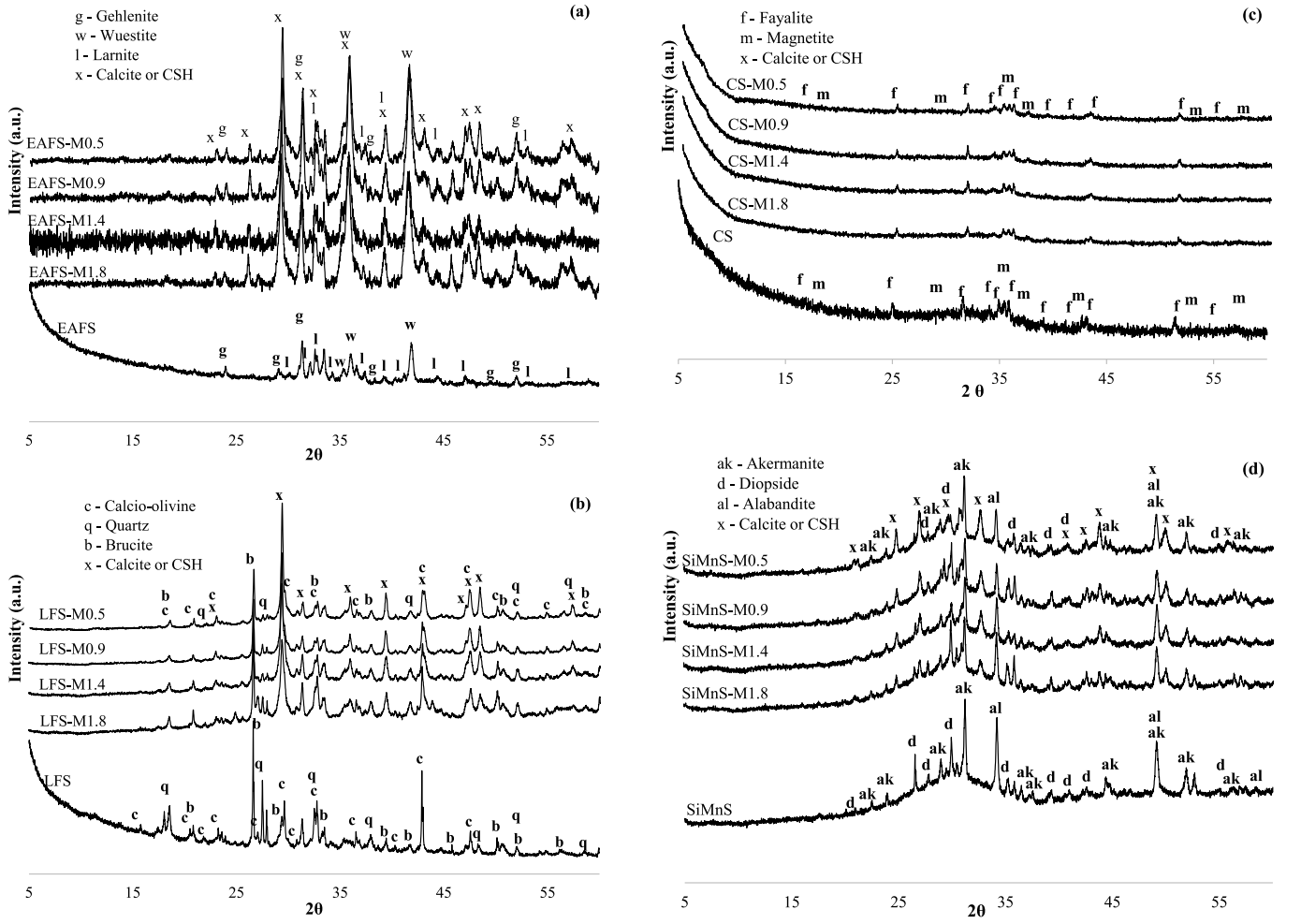

Fig. 13. XRD patterns of the AACs as function of activator module for a curing time of 28 days. (a) EAFS cements and precursor; (b) LFS cements and precursor; (c) CS cements and precursor and (d) SiMnS cements and precursor.

3.5. XRD

The diffraction patterns of the AACs as a function of the activator modulus after 28 days of curing for each precursor used are shown in Fig. 13. It can be observed that the XRD pattern of the AACs using EAFS as precursor present the diffraction peaks corresponding to the crystalline phases wuestite (FeO), gehlenite ($Ca_2Al(SiAl)O_7$) and larnite (Ca_2SiO_4) present in the precursor. In the diffractograms a decrease of the crystalline phases by partial dissolution in the activating solution is observed, appearing a new intense diffraction peak centered at 29.4° that could be associated to the formation of *C*–S–H [93]. In addition, a halo centered at 2θ = 22° ~38° was detected, assigned to amorphous phases, unreacted vitreous phases in the EAFS precursor and the formation of amorphous C(K)-(A)-*S*-H gels [94]. In the AACs using CS as precursor, few changes are observed with respect to the precursor, presenting the diffraction peaks corresponding to fayalite ($(Fe^{2+})2SiO_4$) and magnetite (Fe_3O_4) [29]. This indicates that the crystalline products present in the precursor do not react in the alkaline activation reaction. In AACs employing SiMnS as raw material, a clear hump at 2θ from 20° to 38° is observed in the pattern of all samples, corresponding to the amorphous phase present in the precursor or amorphous *C*-(K)-(A)-*S*-H gels resulting from alkaline activation. The diffraction peaks of the quartz (SiO_2), akermanite ($Ca_2Mg(Si_2O_7)$), diopside ($MgCaSi_2O_6$) and alabandite (MnS) were identified. The diffraction peaks at 34.19° and 49.14° which are indexed into (200) and (220) planes of alabandite (MnS), presents in the precursor are observed with slightly lower intensity indicating partial dissolution and participation in the alkaline activation reaction. The only strong diffraction peaks with a significant change is observed around 29.9° and 32.7°, the former could be assigned to *C*–S–H gel generated during the alkaline activation reaction [95] coincidentally, with the calcite diffraction peaks at 29° and 31°. In the case of AACs using LFS as precursor, peaks present in the precursor were identified, calcio-olivine (Ca_2SiO_4), quartz (SiO_2) and brucite ($Mg(OH)_2$), although new diffraction peaks were observed attributed to calcite. The increase in the intensity of the diffraction peak centered at 29.4° could be due to the presence of unreacted dicalcium silicate because it does not possess hydraulic properties, or the formation of *C*-(A)-*S*-H compounds. A deviation from the baseline is also observed between 20 and 38° assigned to amorphous phases, and the formation of amorphous C(K)-(A)-*S*-H gels.

3.6. SEM-EDX analysis

Fig. 14 shows 500 times magnified SEM images of some AACs. Higher densification is observed when CS and SiMnS nonferrous slags are used as precursors according to the bulk density data. However, a higher amount of shrinkage cracks is observed in the AACs using SiMnS and LFS as precursors.

Fig. 15 shows the 3000 times magnification SEM images and EDX analysis of selected AACs using different ferrous slags, EAFS and LFS as precursors after 28 days of curing. The cements showed heterogeneous morphology and globular nature [61]. It is observed the presence of

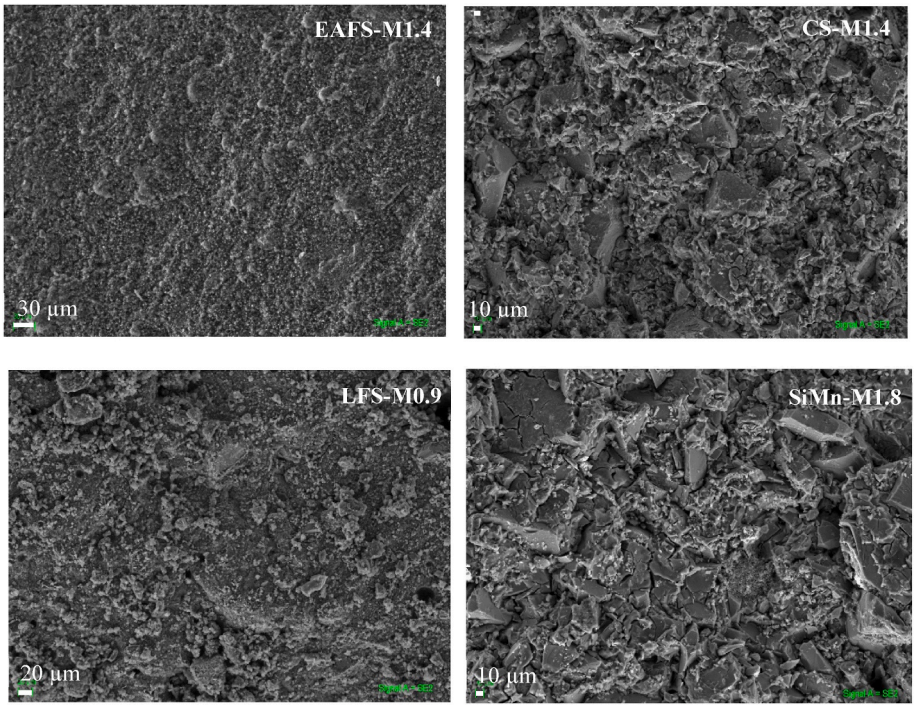

Fig. 14. SEM images of some AACs at 500*x* magnification after 28 days of curing.

lighter particles corresponding to unreacted slag particles (spectra 1 and 3), the gray zone corresponds to the formation of the *C*-(K, Fe)-A-*S*-H gel (spectra 2 and 4) and the darker zones are related to the presence of pores. It can be observed the presence of a higher number of unreacted particles in the AACs using LFS, leading to a lower amount of gel and therefore to lower strengths, according to the results of mechanical properties obtained. In addition, these cements show the presence of microcracks due to expansion reactions due to their high content of free lime and free magnesia.

SEM micrographs at 3000 magnification of the selected AACs after 28 days of curing employing non-ferrous slags as a function of activator modulus are shown in Fig. 16. It can be seen that the morphology of the AACs employing non-ferrous CS and SiMnS slags differs from the morphology of the AACs employing ferrous slags. The microstructure of these AACs is denser although the formation of cracks caused by drying shrinkage and possibly autogenous shrinkage in the curing process, which are embedded with increasing Ms, is observed. In these cements, according to EDX analysis, undissolved slag particles are observed, in higher proportion to lower Ms, which present irregular shapes of different sizes (spectra 1 and 3), surrounded by a binder, amorphous geopolymeric gel K-(Fe)-A-*S*-H in the AACs that use CS and K-(C)–*S*–H gel using SiMnS (spectra 2 and 4) [96]. Other authors indicate the formation of *C*-A-*S*-H gel instead of K-A-*S*-H gel when SiMnS is used [97]. In the studied samples, the formation of a mixed gel is observed. For Ms = 1.8, the formation of a large amount of gel takes place, which reduces the porosity by filling the pores, while causing a significant expansion and the appearance of large microcracks. The lower compressive strength of these AACs may be due to the higher number of cracks that can act as stress concentrators, decreasing mechanical properties of these cements. In the SiMnS-M0.5 binders, crystals in the form of $CaCO_3$ are also observed adhered to the unreacted SiMnS particles according to EDX analysis (Spectrum 5).

4. Conclusions

In this study, different ferrous slags, EAFS and LFS, and non-ferrous slags, CS and SiMnS, have been used in the production of AACs. Although the precursors have different reactive nature, the formation of *C*-(K, Fe)-A-*S*-H gels has been confirmed by FTIR and SEM-EDX analysis in all binders when EAFS and LFS are used as precursor, K-(Fe)-A-*S*-H when CS is used, and K-(C)-A-*S*-H gel in those using SiMnS. Thus, all the precursors used are sufficiently reactive to form AACs. An increase in the modulus of the activator Ms up to 0.9 for LFS cements, up to 1.4 for EAFS and CS cements and up to 1.8 for SiMn cements, resulted in a higher dissolution of reactive species, leading to a higher amount of gel. Lower and higher Ms result in lower amounts of gel due to lower dissolution of reactive species and high dissolution rate which precipitate quickly on the slag grains inhibiting further dissolution, respectively. The flexural and compressive strength followed the trend CS > EAFS > SiMnS > LFS. Thus, optimum values of 7.5 and 51.5 MPa for *C*S-M1.4, 5.7 and 30.5 MPa for EAFS-M1.4, 3.2 and 11.6 MPa for SiMnS-M1.8 and 1.1 and 4.6 MPa for LFS-M0.9 cements are obtained after 28 days of curing. The higher flexural and compressive strengths of the CS cements may be due to higher densification as well as the formation of more geopolymeric gel. In AACs using EAFS, this may be due to the greater amount of amorphous or reactive phase in these slags, as well as the presence of soluble Ca^{2+} ions that favor the formation of *C*-(A)-*S*-H gel that act as nucleation sites and promote to a lesser extent the formation of K-A-*S*-H gel, giving rise to a greater amount of reaction products. Both slags, CS and EAFS, are rich in Fe incorporated in the binder phase contributing to the strength. The lower flexural and compressive strength values of cements using SiMnS as precursor, in the activation conditions used, may be due to the lower gel formation or more hygroscopic gel formation at higher Ms that causes expansion, leading to the appearance of fracture microcracks. While for the AACs using LFS it may be due to the higher crystallinity of the precursor which results in less gel, as well as the presence of free lime and free magnesia which result in microcracks due to expansive reactions.

In view of these results it can be concluded that ferrous and non-ferrous slags can be used as precursors in the manufacture of alkali activated binders. Under the activation conditions studied, the CS and EAFS precursors give rise to more sustainable cements that can have the same applications as Portland cement, including structural applications. While the SiMnS and LFS precursors can be used in the manufacture of

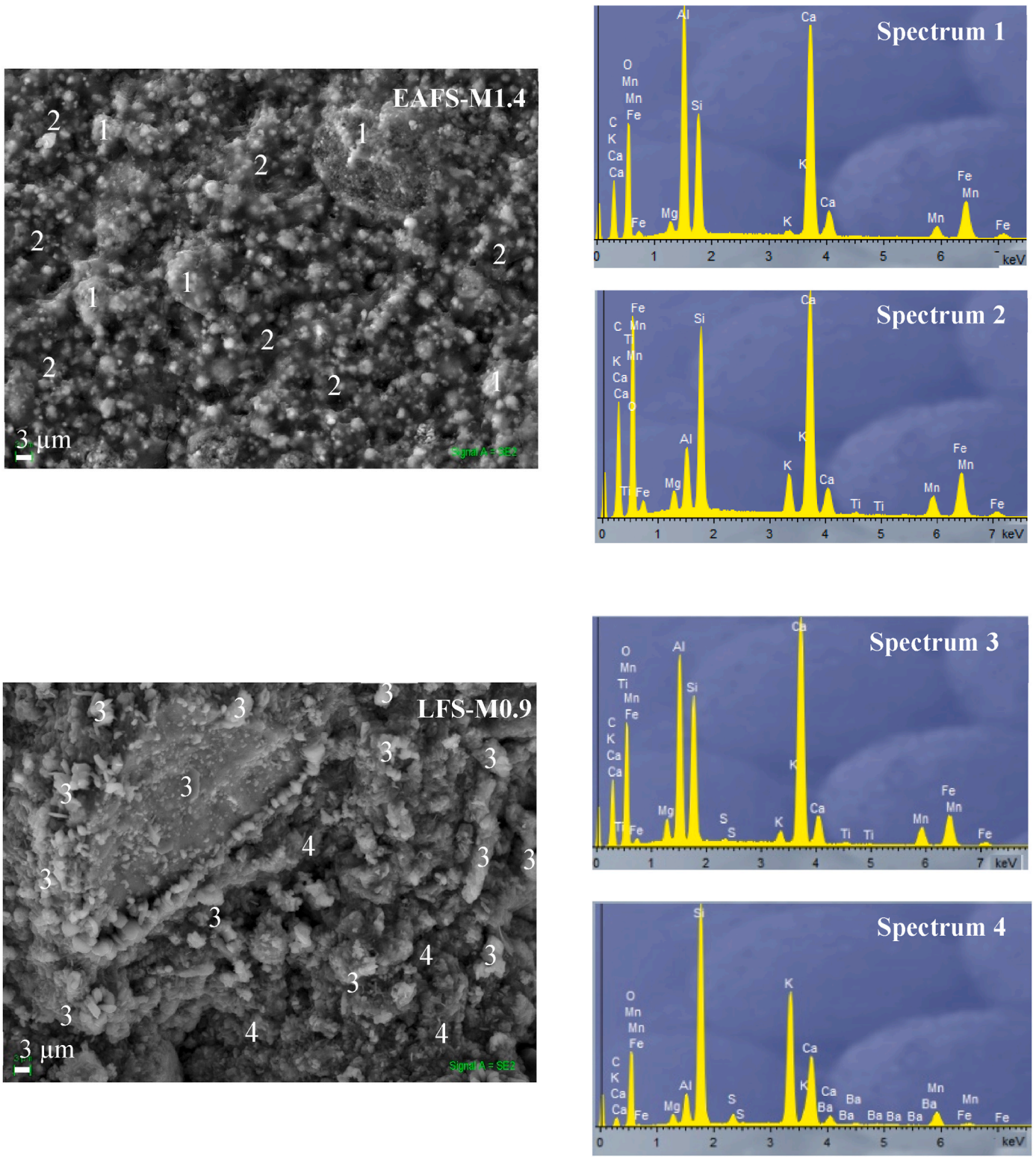

Fig. 15. SEM-EDX analysis of selected AACs using different ferrous slags, EAFS and LFS as precursors at 3000*x* magnification after 28 days of curing.

alkali activated cements with non-structural applications in civil engineering.

CRediT authorship contribution statement

M.A. Gómez-Casero: Conceptualization, Data curation, Formal analysis, Investigation, Methodology, Writing – review & editing. **S. Bueno-Rodríguez:** Conceptualization, Investigation, Writing – review & editing. **E. Castro:** Writing – review & editing. **D. Eliche Quesada:** Conceptualization, Data curation, Formal analysis, Funding acquisition, Investigation, Project administration, Supervision, Writing – original draft, Writing – review & editing.

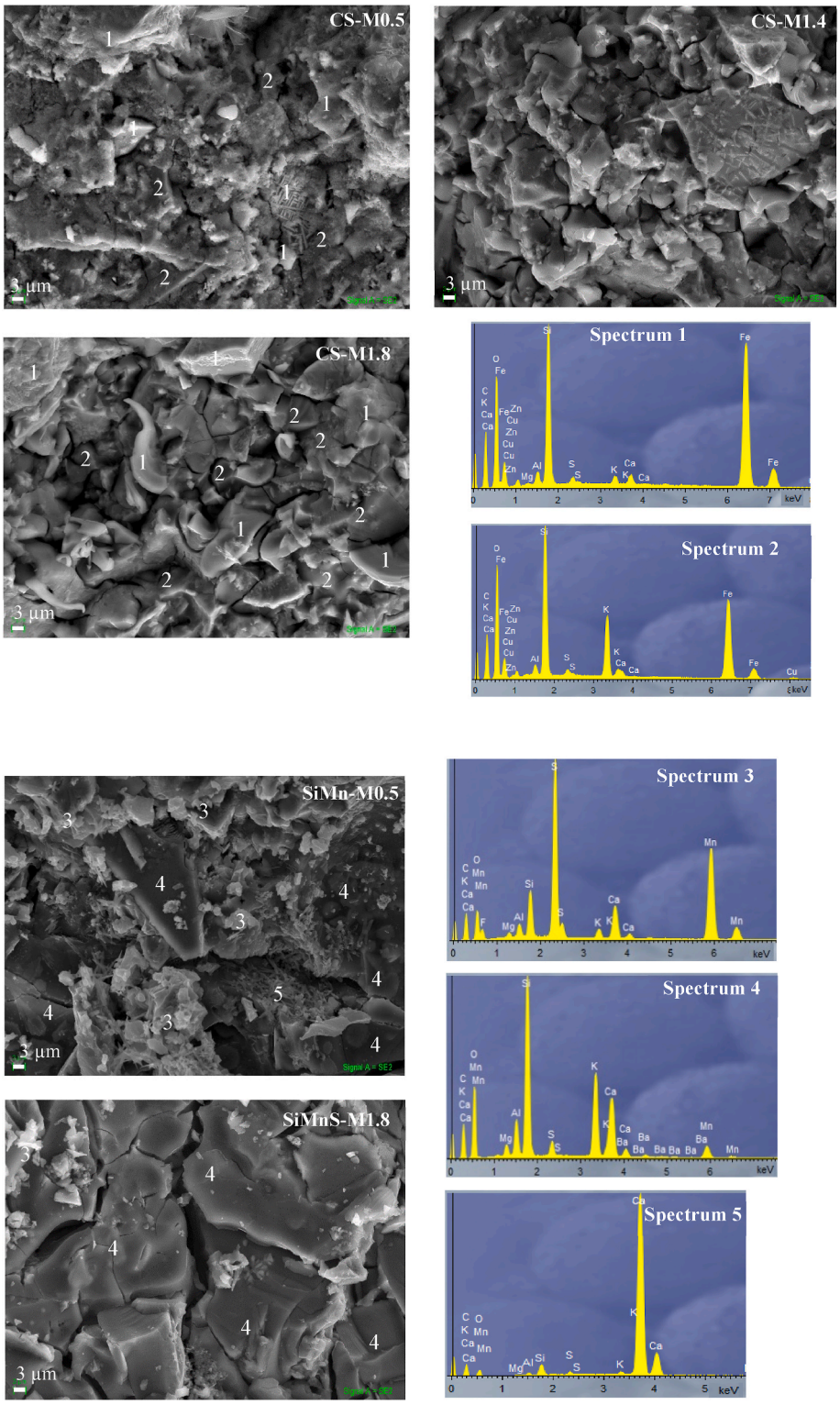

Fig. 16. SEM-EDX analysis of AAC using different non-ferrous slags, CS and SiMnS as precursor as 3000× magnification as function Ms after 28 days of curing.

Declaration of competing interest

The authors declare that they have no known competing financial interests or personal relationships that could have appeared to influence the work reported in this paper.

Data availability

Data will be made available on request.

Acknowledgments

This work has been funded by the project PID2020-115161RB-I00: Applying the circular economy in the development of new low carbon

footprint alkaline activated hydraulic binders for construction solutions (CongActiva), MCIN/AEI/10.13039/501100011033 FEDER "A way of making Europe" and by the project MAT2017-88097-R: Development and characterization of new geopolymeric composites based on waste from the olive industry. Towards a sustainable construction, FEDER/ Ministry of Science, Innovation and Universities, State Research Agency. Authors thank Siderúrgica Sevillana, Atlantic Copper and Ferroatlántica companies for supplying slags. M.A. Gómez-Casero acknowledges support of MINECO (PRE2018-084073). Technical and human support provided by CICT of Universidad de Jaén (UJA, MINECO, Junta de Andalucía, FEDER) is gratefully acknowledged.

References

[1] J. Deja, A. Uliasz-Bochenczyk, E. Mokrzycki, CO_2 emissions from Polish cement industry, Int. J. Greenh. Gas Control 4 (2010) 583–588, https://doi.org/10.1016/j.ijggc.2010.02.002.
[2] J.H. Sharp, C.D. Lawrence, R. Yang, Calcium sulfoaluminate cements-low-energy cements, special cements or what? Adv. Cement Res. 11 (1) (1999) 3–13, https://doi.org/10.1680/adcr.1999.11.1.3.
[3] M.S. Imbabi, C. Carrigan, S. McKenna, Trends and developments in green cement and concrete technology, Int. J. Sustain. Built Environ. 1 (2012) 194–216, https://doi.org/10.1016/j.ijsbe.2013.05.001.
[4] J.L. Provis, Alkali-activated materials, Cement Concr. Res. 114 (2018) 40–48, https://doi.org/10.1016/j.cemconres.2017.02.009.
[5] S.A. Bernal, R. San Nicolas, J.S.J. van Deventer, J.L. Provis, Alkali-activated slag cements produced with a blended sodium carbonate/sodium silicate activator, Adv. Cement Res. 28 (4) (2016) 262–273, https://doi.org/10.1680/jadcr.15.00013.
[6] M. Criado, S.A. Bernal, P. Garcia-Triñanes, J.L. Provis, Influence of slag composition on the stability of steel in alkali-activated cementitious materials, J. Mater. Sci. 53 (2018) 5016–5035, https://doi.org/10.1007/s10853-017-1919-3.
[7] World Steel Association (Ed.): Steel Statistical Yearbook 2019 – Concise Version, Finalized November 2019, (Brussels, Belgium).
[8] UNESID, Asociación de las empresas productoras de acero y de productos de primera transformación del acero de España. https://unesid.org/. (Accessed 13 November 2022).
[9] E. Adesanya, H. Sreenivasan, A.M. Kantola, V.V. Telkki, K. Ohenoja, P. Kinnunen, M. Illikainen, Ladle slag cement-Characterization of hydration and conversion, Construct. Build. Mater. 193 (2018) 128–134, https://doi.org/10.1016/j.conbuildmat.2018.10.179.
[10] European Commision, Reference Document on Best Available Techniques the Cement, Lime and Magnesium Oxide Manufacturing Industries, May 2010.
[11] V.Z. Serjun, B. Mirtič, A. Mladenovič, Evaluation of ladle slag as a potential material or building and civil engineering, Mater Tehnol 47 (2013) 543–550.
[12] L. Valderrama, M. González, S. Santander, B. Zazzali, Recuperación de Cobre Contenido en Escoria de Cobre Mediante Flotación, HOLOS 34 (5) (2018) 40–50, https://doi.org/10.15628/holos.2018.7118.
[13] B. Gorai, R.K. Jana, R.K. Premchand, Characteristics and utilisation of copper slag—a review, Resour. Conserv. Recycl. 39 (2003) 299–313, https://doi.org/10.1016/S0921-3449(02)00171-4.
[14] www.atlantic-copper.es. (Accessed 24 November 2022).
[15] B.R.E.F. Documento, Documento de referencia de Mejores Técnicas Disponibles en la Industria de Procesos de Metales No Férreos, 2005.
[16] C. Shi, C. Meyer, A. Behnood, Utilization of copper slag in cement and concrete, Resour. Conserv. Recycl. 52 (2008) 1115–1120, https://doi.org/10.1016/j.resconrec.2008.06.008.
[17] M. Criado, X. Ke, J.L. Provis, S.A. Bernal, S.A, 7-Alternative inorganic binders based on alkali-activated metallurgical slags, in: H. Savastano Junior, J. Fiorelli, S. F. Dos Santos (Eds.), Sustainable and Nonconventional Construction Materials Using Inorganic Bonded Fiber Composites, Woodhead Publishing, 2017, https://doi.org/10.1016/B978-0-08-102001-2.00008-5.
[18] Engrisa, Analysis of Application of the Concept of End-Of-Waste Status of Electric Arc Furnace Smelting Slag-Carbon Steel, Copper and Silico-Manganese-For Use as an Aggregate (In Bound and Unbound Applications) and Other Uses: as a Raw Material in the Manufactured of Construction Products (Cement and Clinker) and as Abrasive Material, Ministry for Ecological Transition and the Demographic Challenge, Government of Spain, 2021.
[19] CEDEX, Analysis of a Sample of Air-Cooled Silico-Manganese Slag, Convention of Applications in Road Pavements of a Silico-Manganese Slag from Ferroatlántica S. L, 2003.
[20] F. Batista Ribeiro, B. Guida Gouveia, F. Almeida Corrêa do Nascimento, F. Dias Costa, M.A. Vieira da Silva, Characterization of Silicon-Manganese Iron Slag for Employment in Base and Sub-base Layers for Highway, Department of Transportation Engineering, COPPE, Federal University of Rio de Janeiro, Brazil, 2020 adición activa para la fabricación de cementos, https://www.rqueerre.com/construccion/cemex-ferroglobe-caso-practico-de-economia-circular/. (Accessed 2 October 2022).
[21] S.D. Wang, K.L. Scrivener, P.L. Pratt, Factors affecting the strength of alkali-activated slag, Cement Concr. Res. 24 (1994) 1033–1043, https://doi.org/10.1016/0008-8846(94)90026-4.
[22] O. Burciaga-Díaz, J.I. Escalante-García, Structure, Mechanisms of reaction, and strength of an alkali-activated blast-furnace slag, J. Am. Ceram. Soc. 96 (2013) 3939–3948, https://doi.org/10.1111/jace.12620.
[23] M. Ozturk, M. Balcikanli Bankir, O Saltuk Bolukbasi, U. Korkut Sevima, Alkali activation of electric arc furnace slag: mechanical properties and micro analyzes-, J. Build. Eng. 21 (2019) 97–105, https://doi.org/10.1016/j.jobe.2018.10.005.
[24] S. Apithanyasai, P. Nooaek, N. Supakata Apithanyasai, P. Nooaek, N. Supakata, The utilization of concrete residue with electric arc furnace slag in the production of geopolymer bricks, Eng. J. 22 (1) (2018) 1–14, https://doi.org/10.4186/ej.2018.22.1.1.
[25] H. Hafez, D. Kassim, R. Kurda, R. Vasco Silva, J. de Brito, Assessing the sustainability potential of alkali-activated concrete from electric arc furnace slag using the ECO_2 framework, Construct. Build. Mater. 281 (2021) 122559, https://doi.org/10.1016/j.conbuildmat.2021.122559.
[26] B. Xu, Y. Yi, Use of ladle furnace slag containing heavy metals as a binding material in civil engineering, Sci. Total Environ. 705 (2020) 135854, https://doi.org/10.1016/j.scitotenv.2019.135854.
[27] E. Adesanya, K. Ohenoja, P. Kinnunen, M. Illikainen, Alkali activation of ladle slag from steel-making process, J. Sustain. Metall. 3 (2017) 300–310, https://doi.org/10.1007/s40831-016-0089-x.
[28] J. Kuterasińska, A. Król, Mechanical properties of alkali-activated binders based on copper slag, Arch. Civil Eng. Environ. 3 (2015) 61–67.
[29] A. Nazer, J. Payá, M.V. Borrachero, J. Monzó, Use of ancient copper slags in Portland cement and alkali activated cement matrices, J. Environ. Manag. 167 (2016) 115–123, https://doi.org/10.1016/j.jenvman.2015.11.024.
[30] M. Qianmin, D. Haiyun, Z. Xintao, H. Kecheng, L. Zhiwei, Y. Feng, H. Liping, G. Rongxin, Performance of copper slag contained mortars after exposure to elevated temperaturas, Construct. Build. Mater. 172 (2018) 378–386, https://doi.org/10.1016/j.conbuildmat.2018.03.26.
[31] R. Navarro, E. Zornoza, I. Sánchez, E.G. Alcocel, Influence of the type and concentration of the activator on the microstructure of alkali activated SiMn slag pastes, Construct. Build. Mater. 342 (2022) 128067, https://doi.org/10.1016/j.conbuildmat.2022.128067.
[32] S. Kumara, P. García-Triñanes, A. Teixeira-Pinto, M. Bao, Development of alkali activated cement from mechanically activated silico-manganese (SiMn) slag, Cem. Concr. Compos. 40 (2013) 7–13, https://doi.org/10.1016/j.cemconcomp.2013.03.026.
[33] R. Navarro, E. Zornoza, P. Garcés, I. Sánchez, E.G. Alcocel, Optimization of the alkali activation conditions of ground granulated SiMn slag, Construct. Build. Mater. 150 (2017) 781–791, https://doi.org/10.1016/j.conbuildmat.2017.06.064.
[34] M.A. Gómez-Casero, L. Pérez-Villarejo, P.J. Sánchez-Soto, D. Eliche-Quesada, Comparative study of alkali activated cements based on metallurgical slags, in terms of technological properties developed, Sustain Chem Pharm 29 (2022) 100746, https://doi.org/10.1016/j.scp.2022.100746.
[35] H. Jansson, D. Bernin, K. Ramser, Silicate species of water glass and insights for alkali-activated green cement, AIP Adv. 5 (2015) 067167, https://doi.org/10.1063/1.4923371.
[36] ASTM C1437-20. Standard Test Method for Flow of Hydraulic Cement Mortar.
[37] H.-L. Chiang, C. Huang, P. Chiang, The surface characteristics of activated carbon as affected by ozone and alkaline treatment, Chemosphere 47 (3) (2002) 257–265, https://doi.org/10.1016/S0045-6535(01)00215-6.
[38] UNE-EN 1015-11:2000/A1, Methods of Test for Mortar for Masonry - Part 11: Determination of Flexural and Compressive Strength of Hardened Mortar, 2007.
[39] UNE-EN 1015-10, Methods of Test for Mortar for Masonry - Part 10: Determination of Dry Bulk Density of Hardened Mortar, 2000.
[40] ISO-8302, Thermal Insulation - Determination of Steady-State Thermal Resistance and Related Properties - Guarded Hot Plate Apparatus, 1991.
[41] M. Zhang, T. El-Korchi, G. Zhang, J. Liang, M. Tao, Synthesis factors affecting mechanical properties, microstructure, and chemical composition of red mud-fly ash based geopolymers, Fuel 134 (2014) 315–325, https://doi.org/10.1016/j.fuel.2014.05.058.
[42] T. Yang, Z. Zhang, H. Zhu, X. Gao, C. Dai, Q. Wu, Re-examining the suitability of high magnesium nickel slag as precursors for alkali-activated materials, Construct, Build Mater 213 (2019) 109–120, https://doi.org/10.1016/j.conbuildmat.2019.04.063.
[43] M. Teixeira Marvila, A.R. Garcez Azevedo, C.M. Fontes Vieira, Reaction mechanisms of alkali-activated materials, IBRACON Estrut. Mater. 14 (2021) e14309, https://doi.org/10.1590/S1983-41952021000300009.
[44] M.Teixeira Marvila, A.R. Garcez Azevedo, P.R. de Matos, S. Neves Monteiro, C. M. Fontes Vieira, Rheological and the fresh state properties of alkali-activated mortars by blast furnace slag, Materials 14 (8) (2021) 2069, https://doi.org/10.3390/ma14082069.
[45] V. Ponomar, J. Yliniemi, E. Adesanya, K. Ohenoja, M. Illikainen, An overview of the utilisation of Fe-rich residues in alkali-activated binders: mechanical properties and state of iron, J. Clean. Prod. 330 (2022) 129900, https://doi.org/10.1016/j.jclepro.2021.129900.
[46] R.M. Cornell, U. Schwertmann, in: Co KGaA (Ed.), The Iron Oxides: Structure, Properties, Reactions, Occurrences and Uses, second ed., WILEY-VCH GmbH, 2003 https://doi.org/10.1002/3527602097. WILEY-VCH.
[47] L. Weng, K. Sagoe-Crentsil, T. Brown, S. Song, Effects of aluminates on the formation of geopolymers, Mater. Sci. Eng. B Solid-State Mater. Adv. Technol. 117 (2005) 163–168, https://doi.org/10.1016/j.mseb.2004.11.008.
[48] N.M. Piatak, M.B. Parsons, R.R. Seal, Characteristics and environmental aspects of slag: a review, Appl. Geochem. 57 (2015) 236–266, https://doi.org/10.1016/j.apgeochem.2014.04.009.

[49] S. Simon, G.J.G. Gluth, A. Peys, S. Onisei, D. Banerjee, Y. Pontikes, The fate of iron during the alkali-activation of synthetic (CaO-)FeOx-SiO2 slags: an Fe K-edge XANES study, J. Am. Ceram. Soc. 101 (2018) 2107–2118, https://doi.org/10.1111/jace.15354.

[50] B. Mast, A. Cambriani, A.P. Douvalis, Y. Pontikes, W. Schroeyers, B. Vandoren, S. Schreurs, The effect of high dose rate gamma irradiation on the curing of CaO-Fe_xO_y-SiO_2 slag based inorganic polymers: mechanical and microstructural analysis, J. Nucl. Mater. 539 (2020) 152237, https://doi.org/10.1016/j.jnucmat.2020.152237.

[51] C.K.K. Yip, G.C. Lukey, J.L. Provis, J.S.J. van Deventer, Effect of calcium silicate sources on geopolymerisation, Cem.Concr.Res. 38 (2008) 554–564, https://doi.org/10.1016/j.cemconres.2007.11.001.

[52] I. Niklioć, S. Marković, I. Janković - Častvan, V.V. Radmilović, Lj Karanović, Biljana Babić, V.R. Radmilović, Modification of mechanical and thermal properties of fly ash-based geopolymer by the incorporation of steel slag, Mater. Lett. 176 (2016) 301–305, https://doi.org/10.1016/j.matlet.2016.04.121.

[53] J. Temuujin, A. van Riessen, R. Williams, Influence of calcium compounds on the mechanical properties of fly ash geopolymer pastes, J. Hazard Mater. 167 (2009) 82–88, https://doi.org/10.1016/j.jhazmat.2008.12.121.

[54] K. Dombrowski, A. Buchwald, M. Weil, The influence of calcium content on the structure and thermal performance of fly ash based geopolymers, J. Mater. Sci. 42 (2007) 3033–3043, https://doi.org/10.1007/s10853-006-0532.

[55] C. Shi, Characteristics and cementitious properties of ladle slag fines from steel production, Cement Concr. Res. 32 (2002) 459–462, https://doi.org/10.1016/S0008-8846(01)00707-4.

[56] I.Z. Yildirim, M. Prezzi, Chemical, mineralogical, and morphological properties of steel slag, Adv. Civ. Eng. (2011) 463638, https://doi.org/10.1155/2011/463638, 2011.

[57] R. Lloyd, J. Provis, J. Van Deventer, Microscopy and microanalysis of inorganic polymer cements. 2: the gel binder, J. Mater. Sci. 44 (2009) 620–631, https://doi.org/10.1007/s10853-008-3078-z.

[58] P. Chindaprasirt, T. Chareerat, S. Hatanaka, T. Cao, High-strength geopolymer using fine high-calcium fly ash, J. Mater. Civ. Eng. 23 (3) (2011) 264–270, https://doi.org/10.1061/(ASCE)MT.1943-5533.0000161.

[59] S.M. Park, J.G. Jang, N.K. Lee, H.K. Lee, Physicochemical properties of binder gel in alkali-activated fly ash/slag exposed to high temperatures, Cement Concr. Res. 89 (2016) 72–79, https://doi.org/10.1016/j.cemconres.2016.08.004.

[60] F. Pacheco-Torgal, J.A. Labrincha, C. Leonelli, A. Palomo, P. Chindaprasirt, Handbook of Alkali-Activated Cements, Mortars and Concretes, Elsevier Ltd, Cambridge, UK, 2015, https://doi.org/10.1016/C2013-0-16511-7.

[61] P. Duxson, J.L. Provis, G.C. Lukey, S.W. Mallicoat, W.M. Kriven, J.S.J. Van Deventer, Understanding the relationship between geopolymer composition, microstructure and mechanical properties, Colloids Surf., A 269 (2005) 47–58, https://doi.org/10.1016/j.colsurfa.2005.06.060.

[62] M. Criado, A. Fernández-Jiménez, A. Palomo, I. Sobrados, J. Sanz, Effect of the SiO_2/Na_2O ratio on the alkali activation of fly ash. Part II:29Si MAS-NMR Survey, Microporous Mesoporous Mater. 109 (2008) 525–534, https://doi.org/10.1016/j.micromeso.2007.05.062.

[63] L. Fernandez-Carrasco, A. Fernandez Jimenez, A. Palomo, Alkali activation of pozzolan-cement aluminate cement mixtures, in: 12th International Congress on the Chemistry of Cements, 2007.

[64] S. Caijun, L. Yinyu, Investigation on some factors affecting the characteristics of alkali-phosphorus slag cement, Cement Concr. Res. 19 (1989) 527–533, https://doi.org/10.1016/0008-8846(89)90004-5.

[65] S. Apithanyanyasai, N. Supakata, S.J.H. Papong, The potential of industrial waste: using foundry sand with fly ash and electric arc furnace slag for geopolymer brick production, Helyon 6 (3) (2020) e03697, https://doi.org/10.1016/j.heliyon.2020.e03697.

[66] L. Zheng, W. Wang, Y. Shi, The effects of. alkaline dosage and Si/Al ratio on the immobilization of heavy metals in municipal solid waste incineration fly ash-based geopolymer, Chemosphere 79 (6) (2010) 665–671, https://doi.org/10.1016/j.chemosphere.2010.02.018.

[67] R.A. Gado, M. Hebda, M. Lach, J. Mikula, Alkali activation of waste clay bricks: influence of the silica modulus, SiO_2/Na_2O, H_2O/Na_2O molar ratio, and liquid/solid ratio, Materials 13 (2020) 383, https://doi.org/10.3390/ma13020383.

[68] C.K. Yip, G.C. Lukey, J.S.J. van Deventer, The coexistence of geopolymeric gel and calcium silicate hydrate at the early stage of alkaline activation, Cement Concr. Res. 35 (2005) 1688–1697, https://doi.org/10.1016/j.cemconres.2004.10.042.

[69] E. Deira, B.S. Gebregziabiher, S. Peethamparan, Influence of starting material on the early age hydration kinetics, microstructure and composition of binding gel in alkali activated binder systems, Cem. Concr. Compos. 48 (2014) 108–117, https://doi.org/10.1016/j.cemconcomp.2013.11.010.

[70] J. Singh, S.P. Singh, Development of alkali-activated cementitious material using copper slag, Construct. Build. Mater. 211 (2019) 73–79, https://doi.org/10.1016/j.conbuildmat.2019.03.233.

[71] T. Ye, J. Xiao, Z. Duan, S. Li, Geopolymers made of recycled brick and concrete powder – a critical review, Construct. Build. Mater. 330 (2022) 127232, https://doi.org/10.1016/j.conbuildmat.2022.127232.

[72] F. Ameri, P. Shoaei, H. Reza Musaeei, S. Alireza Zareei, Ch Chee Ban, Partial replacement of copper slag with treated crumb rubber aggregates in alkali-activated slag mortar, Construct. Build. Mater. 256 (2020) 119468, https://doi.org/10.1016/j.conbuildmat.2020.119468.

[73] M. Ozturk, M. Balcikanli, B. Omer, S. Bolukbasi, U. Korkut Sevim, Alkali activation of electric arc furnace slag: mechanical properties and micro analyses, J. Build. Eng. 21 (2019) 97–105, https://doi.org/10.1016/j.jobe.2018.10.005.

[74] I. Nikolić, D. Đurović, S. Marković, L. Veselinović, I. Janković-Častvan, V. V. Radmilović, V.R. Radmilović, Alkali activated slag cement doped with Zn-rich electric arc furnace dust, J. Mater. Res. Technol. 9 (2020) 12783–12794, https://doi.org/10.1016/j.jmrt.2020.09.024.

[75] Zh Su, Z. Liu, H. Wang, Sh Xu, D. Wang, F. Han, Reaction kinetics, microstructure and phase evolution of alkali-activated Si-Mn slag during early age, Construct. Build. Mater. 333 (2022) 127437, https://doi.org/10.1016/j.conbuildmat.2022.127437.

[76] S. Kumara, P. García-Triñanes, A. Teixeira-Pinto, M. Bao, Development of alkali activated cement from mechanically activated silico-manganese (SiMn) slag, Cem. Concr. Compos. 40 (2013) 7–13, https://doi.org/10.1016/j.cemconcomp.2013.03.026.

[77] E. Adesanya, K. Ohenoja, P. Kinnunen, M. Illikainen, Alkali activation of ladle slag from steel-making process, J. Sustain. Metall. 3 (2017) 300–310, https://doi.org/10.1007/s40831-016-0089-x.

[78] B. Xu, Y. Yi, Use of ladle furnace slag containing heavy metals as a binding material in civil engineering, Sci. Total Environ. 705 (2020) 135854, https://doi.org/10.1016/j.scitotenv.2019.135854.

[79] W.-Ch Wanga, H.-Y. Wang, H.-Ch Tsai, Study on engineering properties of alkali-activated ladle furnace slag geopolymer, Construct. Build. Mater. 123 (2016) 800–805, https://doi.org/10.1016/j.conbuildmat.2016.07.068.

[80] S.K. Amin, S. El–Sherbiny, A.A. El–Magd, A. Belal, M.J.C. Abadir, Fabrication of geopolymer bricks using ceramic dust waste, Construct. Build. Mater. 157 (2017) 610–620, https://doi.org/10.1016/j.conbuildmat.2017.09.052.

[81] K. Zulkifly, H. Cheng-Yong, L. Yun-Ming, M.M. Al Bakri Abdullah, O. Shee-Ween, Mo S. Bin Khalid, Effect of phosphate addition on room-temperature-cured fly ash-metakaolin blend geopolymers, Construct. Build. Mater. 270 (2021) 121486, https://doi.org/10.1016/j.conbuildmat.2020.121486.

[82] J. Yuan, P. He, D. Jia, Ch Yang, Y. zhang, Sh Yan, Z. Yang, X. Duan, S. Wang, Y. uZhou, Effect of curing temperature and SiO_2/K_2O molar ratio on the performance of metakaolin-based geopolymers, Ceram. Int. 42 (2016) 16184–16190, https://doi.org/10.1016/j.ceramint.2016.07.139.

[83] M. Darder, Y. Gonzalez-Alfaro, P. Aranda, E. Ruiz-Hitzky, Silicate-based multifunctional nanostructured materials with magnetite and Prussian blue: application to cesium uptake, RSC Adv. 4 (2014), https://doi.org/10.1039/C4RA06023G, 35415e35421.

[84] H. Roggendorf, W. Grond, M. Hurbanic, Structural characterization of concentrated alkaline silicate solutions by 29 Si-NMR spectroscopy, FT-IR spectroscopy, light scattering, and electron microscopy - molecules, colloid, and dissolution artefacts, Glastech. Ber. Glass Sci. Technol. 69 (7) (1996) 216–231.

[85] L. Fernández-Carrasco, D. Torrens-Martín, L.M. Morales, S. Martínez-Ramírez, Infrared spectroscopy in the analysis of building and construction materials, in: T. Theophile (Ed.), Infrared Spectroscopy – Materials Science, Engineering and Technology, InTech, 2012, pp. 369–382.

[86] S. Onisei, K. Lesage, B. Blanpain, Y. Pontikes, Early age microstructural transformations of an inorganic polymer made of fayalite slag, J. Am. Ceram. Soc. 98 (2015) 2269–2277, https://doi.org/10.1111/jace.13548.

[87] H. Zhang, W. Chai, Y. Cao, Flotation separation of quartz from gypsum usingbenzyl quaternary ammonium salt as collector, Appl. Surf. Sci. 576 (2022) 151834, https://doi.org/10.1016/j.apsusc.2021.151834.

[88] M. Salman, Ö. Cizera, Y. Pontikes, R. Snellings, L. Vandewalle, B. Blanpain, K. VanBalena, Cementitious binders from activated stainless steel refining slag and the effect of alkali solution, J. Hazard Mater. 286 (2015) 211–219, https://doi.org/10.1016/J.JHAZMAT.2014.12.046.

[89] S. Puligilla, P. Mondal, Co-existence of aluminosilicate and calcium silicate gel characterized through selective dissolution and FTIR spectral subtraction, Cement Concr. Res. 70 (2015) 39–49, https://doi.org/10.1016/J.CEMCONRES.2015.01.006.

[90] Y. Ping, R.J. Kirkpatrick, P. Brent, P.F. McMillan, X. Cong, Structure of calcium silicate hydrate (c-s-h): near-, mid-, and far-infrared spectroscopy, J. Am. Ceram. Soc. 82 (1999) 742–748, https://doi.org/10.1111/J.1151-2916.1999.TB01826.X.

[91] A. Peys, A.P. Douvalis, V. Hallet, H. Rahier, B. Blanpain, Y. Pontikes, Inorganic polymers from CaO-FeOx-SiO2 slag: the start of oxidation of Fe and the formation of a mixed valence binder, Front. Mater. 6 (2019) 1–10, https://doi.org/10.3389/fmats.2019.00212.

[92] M.N. Mužek, J. Zelić, D.J.C. Jozić, Microstructural characteristics of geopolymers based on alkali-activated fly ash, Chem. Eng. J. Biochem. Eng. J. 26 (2) (2012) 89–95.

[93] M. Ozturk, M. Balcikanli Bankir, O. Saltuk Bolukbasi, U. Korkut Sevima, Alkali activation of electric arc furnace slag: mechanical properties and micro analyses, J. Build. Eng. 21 (2019) 97–105, https://doi.org/10.1016/j.jobe.2018.10.005.

[94] D. Shi, J. Ye, W. Zhang, Effects of activator content on properties, mineralogy, hydration and microstructure of alkali-activated materials synthesized from calcium silicate slag and ground granulated blast furnace slag, J. Build. 506 Eng. 32 (2020) 101791, https://doi.org/10.1016/j.jobe.2020.101791.

[95] P.Y. He, Y.J. Zhang, H. Chen, H. Chen, L.C. Liu, Development of an eco-efficient $CaMoO_4$/electroconductive geopolymer composite for recycling silicomanganese slag and degradation of dye wastewater, J. Clean. Prod. 208 (2019) 1476–1487, https://doi.org/10.1016/j.jclepro.2018.10.176.

[96] I. Maragkos, I.P. Giannopoulou, D. Panias, Synthesis of ferronickel slag-based geopolymers, Miner. Eng. 22 (2009) 196–2003, https://doi.org/10.1016/j.mineng.2008.07.003.

[97] I. Garcia-Lodeiro, A. Palomo, A. Fernández-Jiménez, D.E. Macphee, Compatibility studies between N-A-S-H and C-A-S-H gels. Study in the ternary diagram Na_2O–CaO–Al_2O_3 –SiO_2 –H_2O, Cement Concr. Res. 41 (2011) 923–931, https://doi.org/10.1016/j.cemconres.2011.05.006.